Influence of species and processing parameters on recovery and content of brain tissue-derived extracellular vesicles

Yiyao Huang[1,2], Lesley Cheng[3], Andrey Turchinovich[4,5], Vasiliki Machairaki[6], Juan C. Troncoso[6,7], Olga Pletniková[7], Norman J. Haughey[6], Laura J. Vella[8,9], Andrew F. Hill[3], Lei Zheng[2,*], Kenneth W. Witwer[1,6,*]

[1] Department of Molecular and Comparative Pathobiology, Johns Hopkins University School of Medicine, Baltimore, Maryland, USA

[2] Department of Laboratory Medicine, Nanfang Hospital, Southern Medical University, Guangzhou, Guangdong, China

[3] Department of Biochemistry and Genetics, La Trobe Institute for Molecular Science, La Trobe University, Bundoora, Australia

[4] Molecular Epidemiology, German Cancer Research Center DKFZ, Heidelberg, Germany

[5] SciBerg e.Kfm, Mannheim, Germany

[6] Department of Neurology, Johns Hopkins University School of Medicine, Baltimore, Maryland, USA

[7] Department of Pathology, Johns Hopkins University School of Medicine, Baltimore, Maryland, USA

[8] The Florey Institute of Neuroscience and Mental Health, The University of Melbourne, Parkville, Australia

[9] Department of Surgery, The University of Melbourne, The Royal Melbourne Hospital, Parkville, Victoria 3050, Australia

***Co-corresponding authors:**

nfyyzhenglei@smu.edu.cn (LZ), kwitwer1@jhmi.edu (KWW)

Abstract

Extracellular vesicles (EVs) are involved in a wide range of physiological and pathological processes by shuttling material out of and between cells. Tissue EVs may thus lend insights into disease mechanisms and also betray disease when released into easily accessed biological fluids. Since brain-derived EVs (bdEVs) and their cargo may serve as biomarkers of neurodegenerative diseases, we evaluated modifications to a published, rigorous protocol for separation of EVs from brain tissue and studied effects of processing variables on quantitative and qualitative outcomes. To this end, size exclusion chromatography (SEC) and gradient density ultracentrifugation were compared as final separation steps in protocols involving stepped ultracentrifugation. bdEVs were separated from brain tissues of human, macaque, and mouse. Effects of tissue perfusion and a model of post-mortem interval (PMI) before final bdEV separation were probed. MISEV2018-compliant EV characterization was performed, and both small RNA and protein profiling were done. We conclude that the modified, SEC-employing protocol achieves EV separation efficiency roughly similar to a protocol using gradient density ultracentrifugation, while decreasing operator time and, potentially, variability. The protocol appears to yield bdEVs of higher purity for human tissues compared with those of macaque and, especially, mouse, suggesting opportunities for optimization. Where possible, perfusion should be performed in animal models. The interval between death/tissue storage/processing and final bdEV separation can also affect bdEV populations and composition and should thus be recorded for rigorous reporting. Finally, different types of EVs obtained through the modified method reported herein display characteristic RNA and protein content that hint at biomarker potential. To conclude, this study finds that the automatable and increasingly employed technique of SEC can be applied to

tissue EV separation, and also reveals more about the importance of species-specific and technical considerations when working with tissue EVs. These results are expected to enhance the use of bdEVs in revealing and understanding brain disease.

Keywords

Extracellular vesicles; brain; central nervous system; tissue preparation; postmortem interval; small RNA sequencing; proteomics; exosomes; neurodegenerative disease

Introduction

Extracellular vesicles (EVs) are nano-sized, lipid bilayer-delimited particles that are released by various cells. They can package and deliver molecules such as RNAs and proteins and are thus involved in multiple physiological and pathological pathways by serving as messengers in cell-to-cell communication. Roles of EVs in the central nervous system (CNS) have now been well established. EVs are released by all neural cells[1-3], including neurons, oligodendrocytes, astrocytes, and microglia. They can carry disease-associated agents such as amyloid-beta (Aβ)[4-7] and tau[6-8] proteins, which may promote neurodegenerative and inflammatory diseases. However, EVs may also exert protective functions in the CNS by distributing anti-inflammatory factors[9-11]. While brain-derived EVs (bdEVs) may leave the brain and betray the state of the CNS as biomarkers in blood and other peripheral fluids, bdEVs are first found in the tissue interstitial space[12] and may be most likely to act locally. The composition of tissue EVs may thus shed light on physiological and pathological mechanisms in the brain. Moreover, bdEVs in tissue could be used to identify reliable cell-specific markers that could then be used to capture specific populations of CNS-origin EVs in the periphery, helping to diagnose and monitor CNS disease.

In separating EVs from post-mortem brain tissue, as from any tissue, it is critical to achieve some degree of tissue disruption while minimizing cellular disruption; to impose one or more EV separation steps to increase purity; and to show that EVs have been enriched with minimal cellular (or other) contamination. If cells are destroyed, intracellular components and artificially produced vesicles may co-isolate with EVs[13]. Gentle tissue separation might include mechanical

(slicing) and enzymatic digestions. However, extensive mincing or grinding/homogenization, as reported in several studies [12, 14-17], may result in non-EV contaminants and challenge the definition of tissue EVs. Following tissue preparation EV separation is done. Reported methods include standard ultracentrifugation (UC)[16], density gradient ultracentrifugation (DGUC)[12-14], chemical separation/precipitation[15, 18,19] or combinations of these techniques. Finally, after separation, thorough characterization of both EVs and potential contaminants is needed, but only some groups consider the latter [13, 14, 17, 20].

Previously, a DGUC method with a triple sucrose cushion was used as a final step in rigorous separation of EVs from brain tissue[13]. By careful characterization of enriched and depleted EV components, the published method was shown to be highly effective at eliminating cellular contaminants that do not have the same density as EVs. The method is thus valuable and effective, but the DGUC step can also be relatively time-consuming[21-23] (at least three hours), requires an operator skilled in preparing density gradients, and for this reason may have some between-run or between-operator variation. We thus queried if size exclusion chromatography (SEC), an automatable and increasingly employed method of EV separation, could be used in place of DGUC to achieve acceptable EV purity. In this study, we applied an SEC-containing protocol to separate EVs from brain tissues of human, macaque, and mouse. We also evaluated the effects of tissue perfusion and post-mortem interval before final bdEV extraction on various parameters of the recovered bdEVs. Small RNA sequencing and proteomics revealed molecular profiles of bdEVs of human and macaque. In summary, this study adds size exclusion to the list

of techniques that can be applied in bdEV separation and evaluates numerous factors affecting bdEV separation from brain of different species.

Results

Protocol comparison: bdEV separation

The tissue processing and bdEV separation protocol previously published by several members of the author team (Vella et al., JEV, 2017)[13] was followed through the 2,000 x g centrifugation step (Figure 1). After enrichment of large EVs (lEVs) by filtration and 10,000 x g centrifugation, supernatant was subjected to SDGU (as previously published) or SEC. Where indicated, SEC fractions were then concentrated by UC or ultrafiltration (UF) (Figure 1).

Comparison of bdEV particle count, morphology, and protein markers in different fractions of SDGU and SEC: human and mouse tissue

Particle yield per 100 mg tissue input (human or mouse) was determined by nanoparticle tracking analysis (NTA). Particle yield was highest for F2 from SDGU and F7-10 from SEC+UC. Particle concentration was below the reliable range of measurement in F3-6 and F11-14 from the SEC+UC method. Particle yield was similar for human and mouse brains (Figure S1A-B). Transmission electron microscopy (TEM) revealed sEV-like cup-shaped oval and round particles ranging in diameter from 50-200 nm in SDGU fractions (Figure S1C) and F7-10 from SEC+UC (Figure S1D).

Presence of EV-enriched membrane (CD9, CD63, CD81) and cytosolic (TSG101, syntenin) markers, and expected EV-depleted cellular markers (GM130, calnexin, BiP) was examined by Western blot for EV fractions as well as brain homogenate (BH), including BH treated with collagenase (BHC). For human brain-derived EVs, abundant CD63 and CD81 levels were observed in F2 and F3 from SDGU and F7-10 from SEC+UC, while F11-14 (SEC) were positive for CD63 but not CD81. Compared with sEVs, lEVs had lower but still detectable CD63 and CD81. bdEVs from human

samples generally did not have detectable calnexin or GM130, in contrast with the source BH and BHC (Figure S1E-F). However, mouse bdEVs retained some amount of cellular markers regardless of separation technique (Figure S1G-H). Additionally, some apparent differences between EV markers in the different fractions were also observed between human and mouse.

Characterization of human bdEVs obtained by three combinations of methods

Based on the results above, we focused on F2 of SDGU and F7-10 of SEC and examined the output of SDGU compared with SEC+UC and SEC+UF. In these experiments, NTA suggested that the SEC methods yielded a slightly higher number of particles as compared with SDGU (Figure 2A). TEM revealed particles consistent with EV morphology ranging in diameter from 50-200 nm from all methods (Figure 2B). There was no significant protein concentration difference of sEVs obtained by the three methods (Figure 2C), but particle:protein ratio, often used as a surrogate of EV preparation purity, was highest for the SEC + UC methods (Figure 2D). Particles defined as lEVs were indeed larger on average by TEM and contained less CD63 and CD81 than sEVs. They also had lower particle:protein ratios than SEC-purified sEVs.

In terms of putatively EV-enriched and -depleted markers, all methods were consistent with EV marker enrichment and cellular marker depletion (Figure 2E). A small amount of calnexin was found in an SEC+UF lane, though, possibly consistent with the TEM results indicating retention of some fragments by UF. We concluded from these results that, following SEC, UC may have a slight advantage in increasing purity compared with UF.

Comparison of methods for murine bdEV separation

We next applied the same methods to mouse brain. Since our preliminary results indicated more contamination of mouse bdEVs with cellular markers, we also added a fourth method, in which both SEC and SDGU were used. Yield of particles was highest for the SEC+UF combination (Figure 3A), while there were no significant differences in protein yield (Figure 3B). Purity, as estimated by particle:protein ratio, was highest for SEC+UF, then SEC+SDGU and SEC + UC, while SDGU was the lowest (Figure 3C). However, particles obtained by SEC+UF included more non-vesicular material, suggesting again that concentration by UC also served a purification function relative to UF (Figure 3D). However, cellular markers GM130, Calnexin, and Bip were found despite method (Figure S1G, H, Figure S2). Interestingly, in contrast with the human brain results, the particle concentration of bd-lEVs was higher than that of sEVs, and protein content was also higher, contributing to a moderate particle/protein ratio compared with sEVs (Figure 3A-C). As expected, lEVs were larger by TEM (Figure 3D) and included a large number of cellular proteins (Figure S1G,H, Figure S2).

Does PBS perfusion at necropsy affect bdEV separation?

Considering the large amount of cellular markers detected in bdEV preparations from mouse, we reasoned that tissue preparation might be altered to reduce this influence. For example, in animal models, it is often possible to perfuse with buffer (such as PBS) at necropsy, flushing blood from the tissues. We thus separated bdEVs from tissue of animals perfused or not with PBS. Although no remarkable differences were observed for particle or protein yield (Figure 3E), perfusion appeared to reduce the amount of GM130 in bdEVs. However, presence of calnexin and BiP was similar, and apparent changes in some EV-associated proteins were observed (Figure 3F).

What is the effect of post-mortem interval on bdEV separation?

Whereas brain tissue from animal models such as mouse can be processed (or snap-frozen and stored) immediately after necropsy, human brains are acquired, cut, stored, and/or otherwise processed after varying times and incubation temperatures. To assess the influence of one part of the length of time between death and processing (post-mortem interval, PMI), specifically the time after sectioning and before final bdEV extraction, we obtained occipital lobe of macaques that were sacrificed in the course of other studies (the information for used samples sees Table 1). Lobes from the same subject were divided into three parts and incubated at room temperature for two, six, or 24 hours (2, 6, 24H). bdEVs were then obtained using the method ending with SEC+UC as outlined above. bdEVs from tissue incubated for 24H had the highest particle yield (Figure 4A). By TEM, bdEV morphology was the same for macaque as for human and mouse EVs (Figure 4B). In contrast, particle concentration of lEVs did not appear to be affected by the investigated PMI time points (Figure 4A).

Effect of PMI on bdEV small RNA and protein content

Ligation-dependent small RNA sequencing was used to assess the effects of PMI on bdEV small RNA content from tissues of two macaques (Table 1, macaque 3 and 4). Only 2H and 6H libraries were sequenced because quality control electropherograms of sequencing libraries prepared from 24H PMI samples suggested some level of degradation (Figure S3). The mapped read counts were also slightly lower at 6H compared with 2H for both lEVs and sEVs from two macaques (Figure 4C). Strikingly different proportions of RNA biotypes were detected for sEVs and lEVs, but with minimal differences from 2H to 6H (Figure 4D). Prominently, sEVs contained a smaller

percentage of tRNA-related sequences than lEVs. In terms of miRNA diversity, “detected” miRNAs were defined inclusively as those with greater than 5 counts per million mapped reads (CPM). In sEVs, 153 miRNAs were mapped in common for PMI of 2H and 6H, while 147 and 78 miRNAs were detected only at 2H and 6H, respectively. In lEVs, 143 miRNAs were found in common at 2H and 6H, and few miRNAs were detected only at 2H and 6H (Figure 4E). These findings suggest that miRNA diversity may decrease somewhat as PMI increases, perhaps due to degradation.

Because of limited input of macaque protein for proteomics (1 µg), compared with the human studies, only limited number of proteins were identified in sEVs and lEVs from the qualitative proteomics analysis. The number of identified proteins increased for sEVs and lEVs with greater PMI, while it appeared to decrease in BH (Figure S4 A). Almost all sEV and lEV proteins identified at 2H and 6H were also identified at 24H. Many proteins were found only at 24H. 75% of proteins were found at all time points in BH. Moreover, in both BH and EV subtypes, the overlap of proteins at 6H and 24H was greater than that for 2H and 24H, indicating a time-dependent shift in protein detection. Based on pathway involvement, proteins identified in sEVs were especially enriched for known EV (“extracellular exosome”), cytoplasmic, lysosomal, and membrane-associated proteins (Figure S4 B). A stronger enrichment of cytoplasmic components at 24H might indicate more cell disruption in these samples (Figure S4 B). lEVs shared many components with sEVs, but were also enriched for terms such as desmosome and centrosome that did not appear in sEVs. Importantly, though, the meager protein coverage from these samples limits the conclusions we we can draw from the effect of PMI on EV protein content. We also validated the EV-enriched and -depleted markers. Both EV (CD63, CD81, TSG101, syntenin) and cellular

(calnexin) markers were higher at 24H in sEVs (Figure S4C), while CD63 and calnexin were lower at 24H in lEVs.

Small RNA profiling of brain-derived sEVs and lEVs

We next examined small RNA and protein profiles of brain sEVs and lEVs of human and macaque. These included two macaque brains and seven human brains without recorded neurologic or cognitive abnormalities (Table 1, macaque 3 and 4 and Table 2, human 4-10). Total RNA extraction and quality control indicated a slightly higher RNA yield from lEVs compared with sEVs (Figure 5A). Small RNA sequencing revealed a difference in small RNA biotype distribution between BH, lEVs, and sEVs. miRNAs, snoRNAs, and scaRNAs were more enriched in BH, while tRNA fragments were more enriched in lEVs, and rRNA and mRNA fragments in sEVs. Consistent with results for macaque bDEVs (as shown previously in Figure 4D), tRNA and miRNA sequences were enriched in lEVs over sEVs (Figure 5B). The pattern of small RNA expression was thus different not only between BH and EVs overall, but also between sEVs and lEVs (Figure 5C).

For macaque samples, numerous miRNAs were found in lEVs but not in sEVs, while only one miRNA appeared to be detected uniquely in sEVs (Figure 5D). For human samples, 118 miRNAs were detected in common between the two EV classes and BH. All 154 miRNAs found in lEVs but not sEVs were also detected in brain tissue, while additional miRNAs were found in tissue but not EVs (Figure 5D). Normalizing by CPM, among 41 macaque miRNAs found in both lEVs and sEVs, 28 with putative differential abundance were used for unsupervised clustering (Figure 5E, where clusters 1 and 2 are enriched in sEVs and lEVs, respectively). Similarly, unsupervised clustering was done with 48 human miRNAs with fold change >2 between BH and sEV (Figure 5F, where

clusters 1 and 2 are enriched in BH and sEVs, respectively). Interestingly, but perhaps not unexpectedly, lEVs have a miRNA profile different from but intermediate between BH and sEVs. We were also able to identify a small minority of miRNAs that appeared to be enriched in small EVs, with consistency across the two investigated species (Figure 5G).

Proteomic profiling of brain-derived sEVs and lEVs

The same samples were then examined for protein concentration and profile. As expected, for both human and macaque materials, protein concentration decreased from BH to lEVs to sEVs (Figure 6A). For macaque samples, numerous proteins were identified in tissue only, with just a handful identified in sEVs and lEVs (Figure S4 A). The lower proteome coverage is likely due to the lower protein input for macaque EVs. Better coverage was obtained with human samples, for which more protein was available. Proteins identified in samples from at least five donors were included in analysis. 167 proteins (42.2%) were found in both the large and small EVs. Around 45.7% of proteins were detected only in sEVs, 12.1% only in lEVs. 99% of the detected proteome matched entries in existing EV databases Vesiclepedia[35], EVpedia[35], and Exocarta[36]. 71 sEV proteins and 65 lEV proteins were found among the top 100 most commonly reported EV proteins in these databases (Figure 6C, Table 3).

Based on published literature and MISEV2018 suggestions, we examined known markers of cells (focusing on presumably or reportedly “EV-depleted” proteins), EVs, and the central nervous system. For the most part, presumed cellular proteins were enriched in BH, including those associated with mitochondria, ribosomes, nucleus, endoplasmic reticulum (ER), and Golgi (Figure 6D, left panel). Only small amounts of these proteins were found in bdEV preparations; of these,

nuclear proteins were found mostly in lEV preparations, while apolipoprotein D associated with sEVs (Figure 6D). Presumed EV proteins were found in all types of samples (Figure 6D, middle panel) but were almost all enriched in EV preparations. A clear enrichment of certain EV markers was observed for sEVs, including tetraspanins (CD81 and CD9), cytosolic proteins (FLOT1, FLOT2), annexins (ANXA11, ANXA3, ANXA4), RABs (RAB14 and RAB1A) and cytoskeleton proteins (ACTN1). Importantly, bdEVs also carried markers of central nervous system cell types: neurons, microglia, oligodendrocytes, and astrocytes (Figure 6D, right panel). Some of these associations (e.g., for TMEM30A), may suggest selective protein packaging into EVs that could be exploited for selective enrichment of specific bdEV populations from tissue or biofluids. Presence of brain proteins was corroborated by an analysis using the DAVID database, revealing a high enrichment of brain-derived proteins in sEVs (n=264), lEVs (n=179) and BH (n=358) (Figure 6E). Of note, a small number of proteins enriched for terms such as platelet, blood, plasma, T-cell, fibroblast, and erythrocyte may indicate blood cell debris, infiltrating immune cells, or simply non-specificity of some proteins.

GO ontology analyses by STRING and FunRich were used to determine the cellular compartment of proteins recovered from BH and bdEV preparations (Figure 6F). Again, a large portion of proteins associated with both sEVs and lEVs were enriched for EV-related terms like exosomes, vesicle, and cytoplasmic vesicle. The terms membrane, plasma membrane, and whole membrane, instructively, were enriched only for sEVs, while nucleosome, nucleolus, protein containing complex, and intracellular part were enriched only for lEV and BH. Cytoplasm, lysosome, and cytoskeleton were common terms enriched for all groups, while some were exclusively enriched in one group. KEGG and Reactome analyses further confirmed processes related to the CNS,

including synaptic vesicle cycle, axon guidance, neuronal system, and L1CAM interactions, but also identified processes related to metabolism, endocytosis, the immune system, hemostasis, vesicle-mediated transport, membrane trafficking, and signal transduction (Figure 6G).

Discussion

Adapting the protocol previously published by Vella, et al.[13], we evaluated application of SEC to bdEV enrichment from brain tissue. The modified method including SEC achieves a bdEV separation efficiency that may achieve acceptable results compared with SDGU. Furthermore, the modified method decreases operation time after the 10,000 x g centrifugation step from three hours (SDGU spin time) to 15 minutes (SEC on-column collection time), and the SEC step can be almost fully automated, potentially reducing operator variability. We do not suggest that SEC replaces SDGU, which may still be required when the highest levels of purity are needed. Rather, SEC may be an acceptable alternative to process larger numbers of samples or to achieve automation.

Both protocols worked well for human tissues, as assessed by the depletion of "deep cellular" markers. However, for murine and macaque brain in particular, a substantial cellular component was still detected consistently. Since tissue preparation variables might contribute to cellular contamination, we tested for the first time the effects of tissue perfusion and postmortem interval. While perfusion had a noticeable effect in depleting cellular contaminants like GM130, cellular markers were still observed even in bdEVs from PBS-perfused murine brain. Regarding PMI before final bdEV processing, 24 hours of tissue storage resulted in higher particle recovery, but also with a significantly higher number of intracellular proteins in macaque bdEVs. PMI did not substantially change the RNA biotypes of macaque bdEVs, but some small RNA degradation and lower miRNA diversity was associated with long PMI. On the contrary, we did not observe

significant protein and RNA difference among bdEVs from tissues from humans with different PMI (death to acquisition), possibly indicating tissue fragility differences among species. However, we also used cortical tissues (mostly gray matter) for human, while a more varied mixture of gray matter and white matter is typically present for the much smaller structures that are available for macaque and mouse bdEV preparation. This factory could partly confound species comparisons. We conclude that perfusion is advised if possible (with animal models), and that PMI, storage temperature, and other details about tissue preparation and processing should be recorded and reported when describing bdEV separation. We note that it was recently reported that flotation density gradient separation showed lower detectable intracellular proteins compared with velocity gradients [17]; however, flotation gradients require even more time than velocity SDGU. Since overly aggressive tissue digestion may contribute to release of cellular materials[37], and since tissue structure may vary by species, types and concentrations of enzymes and different incubation times and temperatures should be explored to find the minimal adequate digestion condition for tissues of different organisms as well as different tissue regions.

We would like to point out that our study of PMI is limited. Further studies are needed to understand factors such as: temperature and time of brain in the skull after death and before removal; brain storage parameters before sectioning; and additional storage conditions before bdEV extraction.

Since the study of bdEV small RNAs is still in an early phase[13, 14], we investigated small RNA composition of brain tissue and different sizes of bdEVs. The results, with slightly different composition of large and small bdEVs, suggested that not all small RNAs are uniformly loaded from cells into EVs. Consistent with other reports [13, 38-42], we also found that fragments of rRNA

and tRNA, were more abundant than miRNAs in EVs, even without employing ligation-dependent sequencing library preparation[43]. Although some publications have reported a higher miRNA proportion in EVs [44, 45] than in cells, our results suggested that mapped miRNA reads and diversity gradually decreased from brain homogenate to large EVs and then small EVs. At least as assessed by our library preparation and analysis methods, miRNAs account for less than 1% of small RNA in both human and macaque small bdEVs. Nevertheless, several miRNAs were highly enriched in small versus large EVs and/or tissue. These included miRNAs (miR-423, miR-320a, miR-186, miR-146a, miR-1180, let-7b, and let-7d) that were also reported by Vella, et al., who collected data following DGUC bdEV separation [13]. Additionally, miRNAs such as miR-7, miR-21, miR-1260, miR-146a, and miR-222, were enriched in small over large EVs in both macaque and human datasets. Collectively, these data show that lEVs and sEVs, despite some likely overlap, may harbor different proportions of small RNA including miRNA, which may further differ from the ratios in parent cells. Whether this observation is explained by active packaging/exclusion or passive factors (i.e. average distance of specific RNAs from sites of EV biogenesis) remains unresolved, with evidence for and against active sorting [38, 46 39, 45, 47, 48].

Since numerous publications have reported tissue-derived EVs without thorough protein characterization of EV-depleted cellular markers and specific EV subtype markers[12, 15, 16, 49-52], we compared the BH and bdEV proteomes with established EV-related databases. Substantial concordance between our data and the databases was clear (Tabe 3). However, reduced presence of most cellular proteins in bdEVs compared with BH indicated relatively minimal cell disruption during EV separation. In larger EVs, however, EV markers were found alongside higher levels of histones and other proteins that may have derived from broken nuclei or formation of

amphisomes[40, 53]. Additionally, sensitive proteomics methods indicated several cellular or co-isolate markers, including calnexin, GLIPR2, and ApoD in sEVs, though we did not find Calnexin or GM130 expression by WB. These proteins that are associated with intracellular compartments beyond plasma membrane (PM)/ endosomes[54] may be contaminants, but could also be *bona fide* cargo of small bdEVs[55-59]: calnexin is carried by syncytiotrophoblast EVs with immunoregulatory function in preeclampsia[56], while ApoD transported by astroglial cells can exert neuroprotective effects[58]. Numerous cytosolic, annexin, Rab, and cytoskeleton proteins were also found. We conclude from the endosomal and PM markers that sEVs prepared by our method are a mixture of different subtypes of EVs, including true exosomes and ectosomes/microvesicles[60], accompanied by lower amounts of proteins from other cellular compartments.

We further propose that our dataset from bdEVs can suggest important tools for biomarker discovery and mechanistic studies in neurological disease. For example, capturing bdEVs in peripheral samples can assist with monitoring neuropathological changes in the brain. Recently, L1CAM and NCAM [1, 61, 62] have been used to capture plasma neuron-derived EVs, and GLAST for astrocyte-derived EVs[63]. Our data may suggest additional CNS cell-enriched markers that could be used to capture or characterize bdEVs in the periphery. For example, neuron-specific markers detected here include enolase 2 (ENO2) and vesicle-associated membrane protein 2 (VAMP2). Also, many small RNA and protein components of bdEVs are involved in neuronal functions and neurodegenerative diseases. Of the miRNAs highly enriched in brain-derived sEVs from both human and macaque samples (Figure 5G), miR-21 was reported to have neurotoxic effects in bdEVs in simian immunodeficiency virus (SIV)-induced central nervous system (CNS) disease[14], while miR-7[64], miR-125b[64], and miR-222[65, 66] were up-regulated in brain tissue[64], CSF[66] or

plasma[65] of Alzheimer's disease (AD) patients. Based on protein findings, functional annotations and pathway analyses support contributions to neuronal functions. Tau protein is extensively used as a diagnostic tool for AD dementia[67]. TMEM30A interacts with the β carboxyl-terminal fragment of amyloid-β (Aβ) precursor protein in endosomes[68] and is released from the blood-brain barrier[69]. Members of the 14-3-3 protein family and DJ-1 confirm previous findings in CSF derived EVs[70]. We expect that ongoing analyses of these data and future studies of bdEVs from different neurological diseases will yield further insights into mechanisms of neuropathology.

In summary, we characterized bdEVs from human, non-human primate, and mouse tissue harvested under different conditions, testing several variations on EV separation. We hope that this study will add to the growing understanding of the small RNome and proteome composition of bdEVs. We further trust that this study and the associated data will be used to further our knowledge of the regulatory roles of EVs in brain and to facilitate biomarker discovery for neurological diseases.

Methods

Tissue Collection and Preparation

Post-mortem tissues were obtained from separate studies: macaque (Table 1, occipital lobe, perfused, fresh, different post-mortem interval), human (Table 2, Cortex, frozen, Johns Hopkins Alzheimer's Disease Research Center) and mouse (C57BL/6 mice, hemi brains (without the cerebellum and olfactory bulbs), fresh, perfused and non-perfused). All procedures were approved by the Johns Hopkins Univeristy Institutional Review Board (human samples) or the Johns Hopkins University Institutional Animal Care and Use Committee (IACUC, animal studies) and conducted in accordance with the Weatherall Report, the Guide for the Care and Use of Laboratory Animals, and the USDA Animal Welfare Act. For macaque, fresh occipital lobes was divided into three pieces and stored in Hibernate-E medium (Thermo Fisher A12476-01) for 2 hours, 6 hours, and 24 hours, respectively, at room temperature before EV separation to investigate effects of post-mortem interval (PMI) [24]. For mouse, whole brains with or without perfusion with PBS (Thermo Fisher 14190250) through the left ventricle were collected. A total of 50 ml PBS was used for perfusion at a speed of 20 ml/min. Perfused mouse brains were snap frozen on dry ice. All tissues were stored at −80°C before use unless otherwise noted.

Separation of Extracellular Vesicles from Tissue

EVs were separated from tissue using the protocol established previously by Vella, et al, [13] with minor modifications. Before extraction, a small (~50 mg) piece of tissue was stored at −80°C for later protein and RNA extraction. The remaining frozen tissue was weighed and briefly sliced on dry ice and then incubated in 75 U/ml collagenase type 3 (Worthington #CLS-3, S8P18814) in

Hibernate-E solution (human tissue for 20 min, macaque and mouse tissue 15 min, based on previous findings that macaque and mouse brains are more fragile and sensitive to digestion) at 37°C. PhosSTOP and Complete Protease Inhibitor (Sigma-Aldrich PS/PI 4906837001/11697498001) solution was then added to stop digestion. The dissociated tissue was spun at 300 × g for 10 min at 4°C. Small pieces of the pellet ("brain homogenate with collagenase") were stored at −80°C for later protein extraction, while supernatant was transferred to a fresh tube and spun at 2000 × g for 15 min at 4°C. Supernatant was filtered through a 0.22 µm filter (Millipore Sigma, SLGS033SS) for further depletion of tissue debris and spun at 10,000 × g for 30 min at 4°C (AH-650 rotor, Beckman Ultra-Clear Tube with 5 ml capacity). The pellet was resuspended in 100 µl PBS and considered to be "large EVs" (lEVs). The 10,000 × g supernatant was then processed by sucrose DGUC, as previously [13], or SEC followed by concentration by ultracentrifugation or ultrafiltration.

Sucrose Density Gradient Ultracentrifugation (SDGU)

For SDGU, the small EV-containing supernatant from the 10,000 x g step was overlaid on a triple sucrose cushion (F2: 0.6 M, F3: 1.3 M, F4: 2.5 M) and ultracentrifuged for 3 hours at 180,000 × g (average) at 4°C (TH-641 rotor, Thermo Fisher, thinwall polypropylene tube with 13.2 ml capacity) to separate EVs and other particles based on density. After the spin, F1 (1.2ml above F2), F2 and F3 were collected, diluted with PBS, and spun for 70 min at 110,000 x g (average) at 4°C (TH-641 rotor, Thermo Fisher, thinwall polypropylene tube with 13.2 ml capacity) to collect EVs. F2 was defined previously as the EV-enriched fraction [13]. Supernatant was discarded, and the pellet was resuspended in 100 µl PBS.

Size Exclusion Chromatography followed by Ultracentrifugation/Ultrafiltration (SEC and UC / UF)

For SEC, the small EV-containing supernatant from the 10,000 x g step was concentrated with a 100 kilodalton (kDa) molecular weight cut-off (MWCO) protein concentrator (Thermo Fisher 88524) from 5 ml to 0.5 ml before application onto qEV Original SEC columns (IZON Science SP1-USD, Christchurch, New Zealand) that had been pre-rinsed with 15 ml PBS. 0.5 ml fractions were collected by elution with PBS. The first 3 ml (F1-6) eluate was considered the void volume, and a total of 2 ml eluate (Fractions 7-10) were collected and pooled as EV-enriched fractions. The total collection time from SEC columns was around 15 min per sample.

To further purify and concentrate EVs, either ultracentrifugation or ultrafiltration was used. Ultracentrifugation was for 70 min at 110,000 x g (average) at 4°C (TH-641 rotor, Thermo Fisher, thinwall polypropylene tube with 13.2 ml capacity). Supernatant was removed, and the pellet was resuspended in 100 µl PBS. Ultrafiltration was through a 10 kDa MWCO protein concentrator (Thermo Fisher 88516), concentrating the original 2 ml to 100 µl.

Brain homogenate preparation

For protein extraction, brain was processed to brain homogenate (BH) or brain homogenate with collagenase treatment (BHC) by grinding in cold PBS containing PI/PS with a handheld homogenizer (Kontes Pellet Pestle Motor) for 10 s. RIPA lysis buffer (Cell Signaling Technology 9806) was added, and the mixture was sonicated on ice for 2 min. Homogenate was rotated at 4°C for 2 h and spun 15 min at 14,000 x g at 4°C. Supernatant was transferred to tubes and stored at -80°.

For RNA extraction, Trizol (Thermo Fisher 15596018) was added to frozen brain tissue and homogenized with Lysing Matrix D beads (MP Biomedicals 116913100) on using a tissue homogenizer (FastPrep-24, MP Biomedicals).

Nanoparticle Tracking Analysis

Particle size and concentration were measured in scatter mode (488 nm laser) with Particle Metrix ZetaView QUATT® and ZetaView® software version 8.05.10 (Particle Metrix, Germany). EV samples were diluted to a volume of 1 ml and injected into the viewing chamber by syringe. Light scattering was then recorded for 2 minutes with the following settings: Focus: autofocus; Camera sensitivity for all samples: 80.0; Shutter: 70; Scattering Intensity: 4.0; Cell temperature: 25°C. Analysis was done with parameters: Maximum particle size 1000; Minimum particle size 5; Minimum particle brightness 20.

Transmission Electron Microscopy

10 µL EV preparations were adsorbed to glow-discharged 400 mesh ultra-thin carbon coated grids (EMS CF400-CU-UL) for two minutes, followed by 3 quick rinses in TBS and staining in 1% uranyl acetate with 0.05 Tylose. Grids were immediately observed with a Philips CM120 instrument set at 80 kV, and images were captured with an AMT XR80 high-resolution (16-bit) 8-Megapixel camera.

Western Blotting

EV fractions were lysed in 1X RIPA lysis buffer. Protein concentrations were determined by BCA protein assay kit (Thermo Fisher). Equivalent total protein amounts from BH and EVs were

separated on 4−15% stain-free pre-cast SDS-PAGE gradient gels (Bio-Rad) under non-reducing conditions and transferred onto PVDF membranes (Sigma Aldrich). After 1 hour blocking in 5% non-fat milk solution (Bio-Rad 170-6404) at room temperature, membranes were incubated with anti-CD63 (1:1000 dilution), anti-Bip (1:1000 dilution) (BD Biosciences 556019 and 610978, respectively), anti-CD81(1:1000 dilution), anti-Rab27 (1:1000 dilution) (Santa Cruz Biotechnology sc23962, sc74586), anti-TSG101 (1:500 dilution), anti-CD9 (1:500 dilution), anti-Syntenin (1:500 dilution), anti-Calnexin (1:2000 dilution), or anti-GM130 (1:1000 dilution) (the last five antibodies were Abcam ab125011, ab92726, ab133267, ab22595, and ab76154) overnight at 4°C. The membrane was washed 3 times for 8 minutes in PBST while shaking, then incubated with HRP-conjugated secondary antibody (1:10000 dilution) (Santa Cruz Biotechnology sc-2357, sc-516102) at room temperature for 1 hour. After washing again in PBST, the enzyme-linked antibody was detected by incubation with Pico chemiluminescent substrate (Thermo Fisher 34580) and recording on film (Millipore Sigma GE28-9068-38). In some cases, as indicated, total protein was visualized using stain-free gel technology on a ChemiDoc™ Imaging System (Bio-Rad).

RNA extraction and quality control

RNA was extracted by miRNeasy Mini Kit (Qiagen 217004) according to the manufacturer's instructions. EV small RNA size profiles were analyzed using capillary electrophoresis by RNA 6000 Pico Kit (Agilent Technologies 5067-1513) on a Fragment Analyzer (Advanced Analytical). Total RNA and small RNA from BH were analyzed using capillary electrophoresis by RNA 6000 Nano Kit (Agilent Technologies 5067-1511) and RNA 6000 Pico Kit.

Small RNA sequencing

Small RNA libraries were constructed from 50 ng of RNA extracted from brain homogenate or 5 µl of RNA from bdEVs using the Ion Total RNA-Seq Kit V2 (Life Technologies 4475936). Barcoding was performed with the indices from the Ion Xpress™ RNA-Seq Barcode 1-16 Kit (Life Technologies 4471250) according to the manufacturer's protocol and as previously published[25]. The yield and size distribution of the small RNA libraries were assessed using the Agilent 2100 Bioanalyzer™ instrument with DNA 1000 chip (Agilent Technologies 5067-1504). Libraries were prepared for deep sequencing using the Ion Chef system (Life Technologies 4484177) and sequenced on the Ion Torrent S5™ using Ion™ 540 chips (Life Technologies A27765).

Sequencing data analysis

Original BAM files were converted into FASTQ format using picard tools (SamToFastq command). Reads shorter than 15 nt were removed from the raw FASTQ using cutadapt software v1.18. The size-selected reads were aligned to human reference transcriptomes using bowtie software (1 mismatch tolerance) in a sequential manner. Specifically, reads were first mapped to rRNA, tRNA, RN7S, snRNA, snoRNA, scaRNA, VT-RNA, Y-RNA as well as the mitochondrial genome. All reads which did not map to the above RNA species were aligned to human miRNA reference (miRBase 22 release). The remaining reads were further aligned to protein-coding mRNAs and long non-coding RNA (lncRNA) references (GENCODE Release 29). The numbers of reads mapped to each RNA type were extracted using eXpress software based on a previous publication [26]. miRNAs identified with at least 5 reads were used for further analysis. miRNA reads were normalized as reads per million miRNA reads (RPM). Differential gene expression was quantified using R/Bioconductor packages edgeR and limma as described[27]. Hierarchical clustering of miRNAs was performed with Heatmapper[28].

Mass spectrometry

Samples were resuspended in 1 X RIPA buffer (20mM Tris-HCl pH7.5, 150mM NaCl, 1mM Na2EDTA, 1mM EGTA, 1% NP-40, 1% SDS, 2.5mM sodium pyrophosphate, 1mM β-glycerophosphate, 1mM Na3VO4, 1ug/ml leupeptin) and protease inhibitors and incubated on ice for 5 min. The samples were then sonicated for 15 min in an ice water bath before centrifugation at 14,000g at 4°C for 10 min. Protein concentration or the supernatant was determined by Micro BCA assay (Thermo Fisher Scientific 23235). Brain homogenate (3 µg for human, 2 µg for macaque) and 10K pellet and EV samples (2 µg for human, 1 µg for macaque) were buffer exchanged to remove detergent. Protein was resuspended in 8M Urea, 50 mM Tris pH=8.3. 1 µL of TCEP (tris [2-carboxyethyl] phosphine hydrochloride, 200 mM solution in water) was then added to the samples and incubated for 4 hours at 21°C in a ThermoMixer (Eppendorf AG). 4 µL of 1M IAA (iodoacetamide in water) was then added, and samples were incubated in the dark at 21°C. 800 µL of 50 mM Tris (pH 8.3) and 1 µg trypsin were then added to samples prior to overnight incubation at 37°C. 10 µL of 10% trifluoroacetic acid (TFA) was added to each sample to acidify. Samples were cleaned using stage-tips preparations using 3 plugs of Empore polystyrenedivinylbenzene (SBD-XC) copolymer disks (Sigma Aldrich, MO, USA) for solid phase extraction.

Peptides were reconstituted in 0.1% formic acid and 2% acetonitrile and loaded onto a trap column (C18 PepMap 100 µm i.d. × 2 cm trapping column, Thermo Fisher Scientific) at 5 µL/min for 6 min using a Thermo Scientific UltiMate 3000 RSLCnano system and washed for 6 min before switching the precolumn in line with the analytical column (BEH C18, 1.7 µm, 130 Å and 75 µm ID × 25 cm, Waters). Separation of peptides was performed at 45°C, 250 nL/min using a linear

ACN gradient of buffer A (water with 0.1% formic acid, 2% ACN) and buffer B (water with 0.1% formic acid, 80% ACN), starting from 2% buffer B to 13% B in 6 min and then to 33% B over 70 min followed by 50% B at 80 min. The gradient was then increased from 50% B to 95% B for 5 min and maintained at 95% B for 1 min. The column was then equilibrated for 4 min in water with 0.1% formic acid, 2% ACN. Data were collected on a Q Exactive HF (Thermo Fisher Scientific) in Data Dependent Acquisition mode using m/z 350–1500 as MS scan range at 60 000 resolution. HCD MS/MS spectra were collected for the 7 most intense ions per MS scan at 60 000 resolution with a normalized collision energy of 28% and an isolation window of 1.4 m/z. Dynamic exclusion parameters were set as follows: exclude isotope on, duration 30 s and peptide match preferred. Other instrument parameters for the Orbitrap were MS maximum injection time 30 ms with AGC target 3 × 106, MSMS for a maximum injection time of 110 ms with AGT target of 1×10^5.

Proteomics data analysis

Protein sequence data for human (last modified date: 16 May 2019) and pigtailed macaque (last modified date: 26 October 2018) were downloaded from the Uniprot database and used as the database for the search engine. Common Repository of Adventitious Proteins (CRAP) was used as the potential lab contaminant database. Protein identification was performed using the proteomics search engine Andromeda built in to Maxquant V 1.16.0. Trypsin with a maximum of two missed cleavages was used as the cleavage enzyme. Carbamidomethyl of cysteine was set as fixed modification and oxidation of methionine was set as variable modification. The Percolator results were set to reflect a maximum of 1% false discovery rate (FDR). The Label Free quantification was done with match between runs using a match window of 0.7 min. Large LFQ ratios were stabilized to reduce the sensitivity for outliers. For human datasets, data

normalization was done using the Cyclicloess method. For pigtailed macaque, LFQ values were normalized using the delayed normalization described in Cox et al.[29].

Tissue expression data were retrieved using the Database for Annotation, Visualization, and Integrated Discovery (DAVID) [30], while the cellular component annotations of identified proteins were enriched by Funrich[31] and STRING[32]. Kyoto Encyclopedia of Genes and Genomes (KEGG)[33] and Reactome[34] was used to enrich pathway involvement of identified proteins. Statistical significance of enrichment was determined by the tools mentioned above. Only significant categories ($p < 0.05$) were included for analysis.

Statistical analysis

Statistical significance of differences in total EV particle concentration, protein, and particle/protein ratio harvested from different combination of protocols of in Fig. 2 A-C and Fig. 3 A-C were assessed by one-way analysis of variance (ANOVA) with Tukey's multiple comparison test.

Acknowledgments

This work was supported by grants from the US National Institutes of Health (DA040385, DA047807, AI144997, and MH118164, to KWW) and AG057430 (to VM and KWW); by the Michael J. Fox Foundation (to KWW); by UG3CA241694, supported by the NIH Common Fund, through the Office of Strategic Coordination/Office of the NIH Director; and by the National Center for Research Resources and the Office of Research Infrastructure Programs (ORIP) and the National Institutes of Health, grant number P40 OD013117. We thank Suzanne Queen, Brandon Bullock, and Emily Mallick from the Johns Hopkins University School of Medicine for generously providing and processing the non-human primate brain tissues. We thank Connie Talbot, Bob Cole and Tatiana Boronina from the Johns Hopkins University School of Medicine for contributing to proteomics data analysis. We gratefully acknowledge the La Trobe University Comprehensive Proteomics Platform.

Contributions of Authors

K.W.W, Y.H. and L.Z. conceived the idea. Y.H. performed most experiments and drafted the manuscript; K.W.W. directed the project, obtained funding, supervised the experiments, and revised the manuscript; L.C and A.F.H performed small RNA libraries construction, small RNA sequence, mass spectrometry, and proteomics data analysis; A.T. performed small RNA sequencing bioinformatics analysis; V.M., J.C.T, and O.P. processed and provided the human brain samples; N.J.H. provided nanoparticle tracking analysis techniques; L.J.V developed the original protocol and helped with protocol modification. All authors read and approved the final manuscript.

Disclosure of interest

The authors report no conflicts of interest.

Figure Legends

Figure 1. Workflow for brain tissue-derived EV (bdEV) enrichment. Following digestion and differential centrifugation, density gradient ultracentrifugation (DGUC) or SEC was applied to 10,000 x g supernatants to enrich bdEVs (specifically sEVs). The 10,000 x g pellets were collected and defined as the lEV fraction.

Figure 2. Characterization of human bdEVs obtained by three combinations of methods. (A) Particle concentration of human bdEVs separated by three combinations of methods was measured by NTA (Particle Metrix). Particle concentration for each group was normalized by tissue mass (per 100 mg). (B) Protein concentration of human bdEVs separated by different methods and measured by BCA protein assay (per 100 mg tissue). (C) Ratio of particles to protein (particles/μg). (A)-(C): Data are presented as the mean with range. *$p < 0.05$ by two-tailed Turkey's multiple comparison test. (D) bdEVs were visualized by negative staining transmission electron microscopy (scale bar = 100 nm). TEM is representative of five images taken of each fraction from three independent human tissue samples. (E) Western blot analysis of GM130, calnexin, CD81, CD63, and syntenin associated with BH and EV fractions. WB are representative of three independent human tissue EV separations from SDGU and SEC+UC methods, and one independent human tissue EV separation from SEC+UF method.

Figure 3. Characterization of murine bdEVs. (A) Particle concentration of murine bdEVs separated by different methods was measured by NTA (Particle Metrix, normalized per 100 mg tissue). (B) Protein concentration of murine bdEVs separated by different

methods and measured by BCA protein assay kit (per 100 mg tissue). (C) Ratio of particles to protein (particles/μg). (A)-(C): Data are presented as the mean with range. (D) bdEVs were visualized by negative staining transmission electron microscopy (scale bar = 100 nm). TEM is representative of five images taken of each fraction from three independent tissue samples. (E) Particle and protein concentration of murine bd-sEVs from PBS-perfused and non-perfused brains. Data are presented as the mean with range (n = 4). (F) Western blot analysis of GM130, Bip, calnexin, TSG101, syntenin, and CD9 associated with BH and EV fractions from perfused and non-perfused murine brains. WB are representative of three independent murine tissue EV separation from SDGU method.

Figure 4. Effect of postmortem interval on bdEV separation. (A) Particle concentration of bdEV preparations from 2H, 6H and 24H postmortem interval (PMI) macaque brains was measured by NTA (Particle Metrix, normalized per 100 mg tissue). Data are presented as the mean with range (n=4). (B) BdEVs from 2H, 6H and 24H PMI macaque brains were visualized by negative staining transmission electron microscopy (scale bar = 100 nm). TEM is representative of five images taken of each fraction from two independent tissue samples. (C) Small RNA sequencing, total reads from sEVs and lEVs from 2H and 6H PMI (n=2). (D) Average percent (n=2) of mapped reads for the nine most abundant RNA classes in sEVs and lEVs at 2H and 6H PMI. (E) Venn diagram of detected miRNAs (mean reads > five counts per million mapped reads (CPM)) from two independent sEV and lEV preparations at 2H and 6H PMI.

Figure 5. Small RNA profiles of bdEVs from two primate and seven human brain tissues. (A) RNA concentration of lEV and sEV fractions from NHP and human brain. Data are presented as the mean with range. (B) Average percent of mapped reads of the nine most abundant RNA classes in BH, lEVs, and sEVs (human, n=7). (C) Multidimensional scaling analysis based on quantitative small RNA profiles of BH, lEVs and sEVs. (n=2 for NHP, n=7 for human) (D) Venn diagram of miRNAs (mean raw reads greater than 5) in lEVs, sEVs, and BH from non-human primate and human brain (n=2 for NHP, n=7 for human). (E) Unsupervised hierarchical clustering of 28 differentially abundant miRNAs of lEVs and sEVs (NHP, n=2). Cluster 1: enriched in sEVs; Cluster 2: enriched in lEVs. (F) Unsupervised hierarchical clustering of 48 differentially abundant miRNAs (BH vs sEVs, mean fold change > 2; human, n=7). Cluster 1: enriched in BH; Cluster 2: enriched in sEVs. (G) Abundance comparison of five miRNAs enriched in sEVs vs lEVs and/or BH for both primate species.

Figure 6. Protein profiles of EVs from two primate and seven human brain tissues. (A) Protein concentration of BH, lEV, and sEV fractions from NHP and human brain (BCA). (B) Venn diagram of identified proteins in lEVs and sEVs of human (proteins identified in 5 from n=7 individuals). (C) Ven diagram of human EV and lEV proteins matched to the top 100 proteins in EV databases Vesiclepedia, EVpedia, and Exocarta. (D) Enrichment of intracellular, extracellular vesicle (EV) and central nervous system (CNS) proteins in human brain sEV, lEV, and BH preparations. (n=7) (E) Tissue derivation of human BH, lEV, and sEV proteins (DAVID knowledgebase). (F) Cellular compartments of human BH, lEV and sEV proteins (STRING

and FunRich). (G) Pathway involvement of human bd-sEV proteins according to the Kyoto Encyclopedia of Genes and Genomes (KEGG) and Reactome.

Figure S1. Comparison of bdEVs in different fractions of SDGU and SEC: human and mouse brain. (A) Particle concentration of SDGU fractions from human and murine brain by NTA (Particle Metrix). (B) Particle concentration of SEC fractions from human and murine brain (NTA). (A)-(B): Data are presented as the mean with range. (C) Three fractions from SDGU visualized by TEM (scale bar = 100 nm). (D) Fractions 7-10 from SEC (TEM, scale bar = 100 nm). TEM is representative of five images taken of each fraction from three independent human tissue samples. (E) Western blot analysis of calnexin, CD63, TSG101, CD81, and CD9 of brain tissue and SDGU fractions (human) (n=1). (F) Western blot analysis of GM130, calnexin, CD63, syntenin, and CD81 of brain tissue and SEC fractions (human) (n=1). (G) Western blot analysis of GM130, calnexin, Bip, TSG101, syntenin, CD9, and CD81 of brain tissue and SDGU fractions (mouse) (n=1). (H) Western blot analysis of Bip and Rab27a of brain tissue and SEC fractions (mouse) (n=1).

Figure S2. Western blot analysis: murine brain tissue and EV preparations. In each of the following, tissue proteins were compared with EV fractions obtained as indicated. (A) SDGU fractions; immunoblotting for GM130, calnexin, Bip, and TSG101 (n=3). (B) SEC + SDGU and SEC + UF fractions; immunoblotting for calnexin, Bip, and TSG101 (n=1). (C) SEC + UF method fractions; immunoblotting for calnexin, Bip, CD9, and TSG101 (n=2). (D) SEC + UC; immunoblotting for GM130, calnexin, and TSG101 (n=1).

Figure S3. Bioanalyzer analysis of bdEV small RNA libraries. Size distribution of bdEV libraries from 2H, 6H, and 24H postmortem interval (PMI) macaque brains (n=2), measured by Bioanalyzer.

Figure S4. Effect of postmortem interval on bdEV protein contents. (A) Venn diagram of identified protein number of sEVs and lEVs at 2H, 6H, and 24H PMI in either two macaques. (B) Enrichment of cellular compartments of proteins identified in sEVs and lEVs at 2H, 6H, and 24H PMI (FunRich).. (C) Western blot analysis of calnexin, CD63, CD81, TSG101, and syntenin associated with BH and EVs of macaque brain tissue at different PMI. WB are representative of two independent tissue EV separations.

References Cited

1. Fiandaca, M.S. *et al.* Identification of preclinical Alzheimer's disease by a profile of pathogenic proteins in neurally derived blood exosomes: A case-control study. *Alzheimer's & dementia : the journal of the Alzheimer's Association* **11**, 600-607 e601 (2015).
2. Scolding, N.J., Houston, W.A., Morgan, B.P., Campbell, A.K. & Compston, D.A. Reversible injury of cultured rat oligodendrocytes by complement. *Immunology* **67**, 441-446 (1989).
3. Goetzl, E.J. *et al.* Decreased synaptic proteins in neuronal exosomes of frontotemporal dementia and Alzheimer's disease. *FASEB journal : official publication of the Federation of American Societies for Experimental Biology* **30**, 4141-4148 (2016).
4. Rajendran, L. *et al.* Alzheimer's disease beta-amyloid peptides are released in association with exosomes. *Proceedings of the National Academy of Sciences of the United States of America* **103**, 11172-11177 (2006).
5. Sharples, R.A. *et al.* Inhibition of gamma-secretase causes increased secretion of amyloid precursor protein C-terminal fragments in association with exosomes. *FASEB journal : official publication of the Federation of American Societies for Experimental Biology* **22**, 1469-1478 (2008).
6. Winston, C.N. *et al.* Prediction of conversion from mild cognitive impairment to dementia with neuronally derived blood exosome protein profile. *Alzheimer's & dementia (Amsterdam, Netherlands)* **3**, 63-72 (2016).

7. Fiandaca, M.S. *et al.* Identification of preclinical Alzheimer's disease by a profile of pathogenic proteins in neurally derived blood exosomes: A case-control study. *Alzheimer's & dementia : the journal of the Alzheimer's Association* **11**, 600-607.e601 (2015).
8. Saman, S. *et al.* Exosome-associated tau is secreted in tauopathy models and is selectively phosphorylated in cerebrospinal fluid in early Alzheimer disease. *The Journal of biological chemistry* **287**, 3842-3849 (2012).
9. Elia, C.A. *et al.* Intracerebral Injection of Extracellular Vesicles from Mesenchymal Stem Cells Exerts Reduced Abeta Plaque Burden in Early Stages of a Preclinical Model of Alzheimer's Disease. *Cells* **8** (2019).
10. Perez-Gonzalez, R. *et al.* Neuroprotection mediated by cystatin C-loaded extracellular vesicles. *Scientific reports* **9**, 11104 (2019).
11. Bonafede, R. *et al.* Exosome derived from murine adipose-derived stromal cells: Neuroprotective effect on in vitro model of amyotrophic lateral sclerosis. *Experimental cell research* **340**, 150-158 (2016).
12. Perez-Gonzalez, R., Gauthier, S.A., Kumar, A. & Levy, E. The exosome secretory pathway transports amyloid precursor protein carboxyl-terminal fragments from the cell into the brain extracellular space. *The Journal of biological chemistry* **287**, 43108-43115 (2012).
13. Vella, L.J. *et al.* A rigorous method to enrich for exosomes from brain tissue. *Journal of extracellular vesicles* **6**, 1348885 (2017).
14. Yelamanchili, S.V. *et al.* MiR-21 in Extracellular Vesicles Leads to Neurotoxicity via TLR7 Signaling in SIV Neurological Disease. *PLoS pathogens* **11**, e1005032 (2015).
15. Gallart-Palau, X., Serra, A. & Sze, S.K. Enrichment of extracellular vesicles from tissues of the central nervous system by PROSPR. *Molecular neurodegeneration* **11**, 41 (2016).
16. Ngolab, J. *et al.* Brain-derived exosomes from dementia with Lewy bodies propagate alpha-synuclein pathology. *Acta neuropathologica communications* **5**, 46 (2017).
17. Hurwitz, S.N. *et al.* An optimized method for enrichment of whole brain-derived extracellular vesicles reveals insight into neurodegenerative processes in a mouse model of Alzheimer's disease. *Journal of neuroscience methods* **307**, 210-220 (2018).
18. Shin, H. *et al.* High-yield isolation of extracellular vesicles using aqueous two-phase system. *Scientific reports* **5**, 13103 (2015).
19. Loyer, X. *et al.* Intra-Cardiac Release of Extracellular Vesicles Shapes Inflammation Following Myocardial Infarction. *Circulation research* **123**, 100-106 (2018).
20. Polanco, J.C., Scicluna, B.J., Hill, A.F. & Gotz, J. Extracellular Vesicles Isolated from the Brains of rTg4510 Mice Seed Tau Protein Aggregation in a Threshold-dependent Manner. *The Journal of biological chemistry* **291**, 12445-12466 (2016).
21. Chen, B.-Y. *et al.* Advances in exosomes technology. *Clinica Chimica Acta* **493**, 14-19 (2019).
22. Dauros Singorenko, P. *et al.* Isolation of membrane vesicles from prokaryotes: a technical and biological comparison reveals heterogeneity. *Journal of extracellular vesicles* **6**, 1324731 (2017).
23. Van Deun, J. *et al.* The impact of disparate isolation methods for extracellular vesicles on downstream RNA profiling. *Journal of extracellular vesicles* **3**, 10.3402/jev.v3403.24858 (2014).
24. Sampaio-Silva, F., Magalhães, T., Carvalho, F., Dinis-Oliveira, R.J. & Silvestre, R. Profiling of RNA Degradation for Estimation of Post Morterm Interval. *PloS one* **8**, e56507 (2013).
25. Cheng, L. & Hill, A.F. Small RNA Library Construction for Exosomal RNA from Biological Samples for the Ion Torrent PGM and Ion S5 System. *Methods in molecular biology* **1545**, 71-90 (2017).
26. Roberts, A. & Pachter, L. Streaming fragment assignment for real-time analysis of sequencing experiments. *Nature methods* **10**, 71 (2012).
27. Law, C.W. *et al.* RNA-seq analysis is easy as 1-2-3 with limma, Glimma and edgeR. *F1000Research* **5**, ISCB Comm J-1408 (2016).

28. Babicki, S. *et al.* Heatmapper: web-enabled heat mapping for all. *Nucleic acids research* **44**, W147-153 (2016).
29. Cox, J. *et al.* Accurate proteome-wide label-free quantification by delayed normalization and maximal peptide ratio extraction, termed MaxLFQ. *Molecular & cellular proteomics : MCP* **13**, 2513-2526 (2014).
30. Huang da, W., Sherman, B.T. & Lempicki, R.A. Systematic and integrative analysis of large gene lists using DAVID bioinformatics resources. *Nature protocols* **4**, 44-57 (2009).
31. Pathan, M. *et al.* FunRich: An open access standalone functional enrichment and interaction network analysis tool. *Proteomics* **15**, 2597-2601 (2015).
32. Szklarczyk, D. *et al.* STRING v11: protein-protein association networks with increased coverage, supporting functional discovery in genome-wide experimental datasets. *Nucleic acids research* **47**, D607-d613 (2019).
33. Kanehisa, M., Sato, Y., Furumichi, M., Morishima, K. & Tanabe, M. New approach for understanding genome variations in KEGG. *Nucleic acids research* **47**, D590-d595 (2019).
34. Joshi-Tope, G. *et al.* Reactome: a knowledgebase of biological pathways. *Nucleic acids research* **33**, D428-432 (2005).
35. Kalra, H. *et al.* Vesiclepedia: a compendium for extracellular vesicles with continuous community annotation. *PLoS biology* **10**, e1001450 (2012).
36. Keerthikumar, S. *et al.* ExoCarta: A Web-Based Compendium of Exosomal Cargo. *Journal of molecular biology* **428**, 688-692 (2016).
37. Volovitz, I. *et al.* A non-aggressive, highly efficient, enzymatic method for dissociation of human brain-tumors and brain-tissues to viable single-cells. *BMC neuroscience* **17**, 30 (2016).
38. Tosar, J.P. *et al.* Assessment of small RNA sorting into different extracellular fractions revealed by high-throughput sequencing of breast cell lines. *Nucleic acids research* **43**, 5601-5616 (2015).
39. Nolte-'t Hoen, E.N.M. *et al.* Deep sequencing of RNA from immune cell-derived vesicles uncovers the selective incorporation of small non-coding RNA biotypes with potential regulatory functions. *Nucleic acids research* **40**, 9272-9285 (2012).
40. Jeppesen, D.K. *et al.* Reassessment of Exosome Composition. *Cell* **177**, 428-445 e418 (2019).
41. Murillo, O.D. *et al.* exRNA Atlas Analysis Reveals Distinct Extracellular RNA Cargo Types and Their Carriers Present across Human Biofluids. *Cell* **177**, 463-477 e415 (2019).
42. Huang, Y. *et al.* Telepathology consultation for frozen section diagnosis in China. *Diagn Pathol* **13**, 29 (2018).
43. Turchinovich, A. *et al.* Capture and Amplification by Tailing and Switching (CATS). An ultrasensitive ligation-independent method for generation of DNA libraries for deep sequencing from picogram amounts of DNA and RNA. *RNA biology* **11**, 817-828 (2014).
44. Langevin, S.M. *et al.* Balancing yield, purity and practicality: a modified differential ultracentrifugation protocol for efficient isolation of small extracellular vesicles from human serum. *RNA biology* **16**, 5-12 (2019).
45. Li, C. *et al.* Characterization and selective incorporation of small non-coding RNAs in non-small cell lung cancer extracellular vesicles. *Cell & bioscience* **8**, 2 (2018).
46. Squadrito, M.L. *et al.* Endogenous RNAs modulate microRNA sorting to exosomes and transfer to acceptor cells. *Cell reports* **8**, 1432-1446 (2014).
47. Guduric-Fuchs, J. *et al.* Selective extracellular vesicle-mediated export of an overlapping set of microRNAs from multiple cell types. *BMC genomics* **13**, 357 (2012).
48. Ji, H. *et al.* Deep sequencing of RNA from three different extracellular vesicle (EV) subtypes released from the human LIM1863 colon cancer cell line uncovers distinct miRNA-enrichment signatures. *PloS one* **9**, e110314 (2014).

49. Gallart-Palau, X. *et al.* Brain-derived and circulating vesicle profiles indicate neurovascular unit dysfunction in early Alzheimer's disease. *Brain pathology* (2019).
50. Jingushi, K. *et al.* Extracellular vesicles isolated from human renal cell carcinoma tissues disrupt vascular endothelial cell morphology via azurocidin. *International journal of cancer. Journal international du cancer* **142**, 607-617 (2018).
51. Ge, X. *et al.* Circular RNA expression alterations in extracellular vesicles isolated from murine heart post ischemia/reperfusion injury. *International journal of cardiology* (2019).
52. Peng, K.Y. *et al.* Apolipoprotein E4 genotype compromises brain exosome production. *Brain : a journal of neurology* (2018).
53. Fader, C.M., Sánchez, D., Furlán, M. & Colombo, M.I. Induction of autophagy promotes fusion of multivesicular bodies with autophagic vacuoles in K562 cells. *Traffic* **9**, 230-250 (2008).
54. Thery, C. *et al.* Minimal information for studies of extracellular vesicles 2018 (MISEV2018): a position statement of the International Society for Extracellular Vesicles and update of the MISEV2014 guidelines. *Journal of extracellular vesicles* **7**, 1535750 (2018).
55. lotvall, J. Mitochondrial protein enriched extracellularvesicles discovered in human melanoma tissuescan be detected in patient plasma. (2019).
56. Li, H. *et al.* Differential Proteomic Analysis of Syncytiotrophoblast Extracellular Vesicles from Early-Onset Severe Preeclampsia, using 8-Plex iTRAQ Labeling Coupled with 2D Nano LC-MS/MS. *Cellular physiology and biochemistry : international journal of experimental cellular physiology, biochemistry, and pharmacology* **36**, 1116-1130 (2015).
57. Zhou, X. *et al.* Label-free quantification proteomics reveals novel calcium binding proteins in matrix vesicles isolated from mineralizing Saos-2 cells. *Bioscience trends* **7**, 144-151 (2013).
58. Pascua-Maestro, R. *et al.* Extracellular Vesicles Secreted by Astroglial Cells Transport Apolipoprotein D to Neurons and Mediate Neuronal Survival Upon Oxidative Stress. *Frontiers in cellular neuroscience* **12**, 526 (2018).
59. Cheow, E.S. *et al.* Plasma-derived Extracellular Vesicles Contain Predictive Biomarkers and Potential Therapeutic Targets for Myocardial Ischemic (MI) Injury. *Molecular & cellular proteomics : MCP* **15**, 2628-2640 (2016).
60. Witwer, K. & Théry, C. Extracellular vesicles or exosomes? On primacy, precision, and popularity influencing a choice of nomenclature. *Journal of extracellular vesicles* **8**, 1648167 (2019).
61. Kapogiannis, D. *et al.* PATHOGENIC PROTEINS IN NEURALLY-DERIVED BLOOD EXOSOMES AS NEAR-PERFECT DIAGNOSTIC AND PROGNOSTIC BIOMARKERS FOR ALZHEIMER'S DISEASE. *Alzheimer's & Dementia* **10**, P281 (2014).
62. Goetzl, E.J. *et al.* Low neural exosomal levels of cellular survival factors in Alzheimer's disease. *Ann Clin Transl Neurol* **2**, 769-773 (2015).
63. Goetzl, E.J. *et al.* Cargo proteins of plasma astrocyte-derived exosomes in Alzheimer's disease. *FASEB journal : official publication of the Federation of American Societies for Experimental Biology* **30**, 3853-3859 (2016).
64. Pogue, A.I. & Lukiw, W.J. Up-regulated Pro-inflammatory MicroRNAs (miRNAs) in Alzheimer's disease (AD) and Age-Related Macular Degeneration (AMD). *Cellular and molecular neurobiology* **38**, 1021-1031 (2018).
65. Kayano, M. *et al.* Plasma microRNA biomarker detection for mild cognitive impairment using differential correlation analysis. *Biomarker research* **4**, 22 (2016).
66. Dangla-Valls, A. *et al.* CSF microRNA Profiling in Alzheimer's Disease: a Screening and Validation Study. *Molecular neurobiology* **54**, 6647-6654 (2017).
67. Guix, F.X. *et al.* Detection of Aggregation-Competent Tau in Neuron-Derived Extracellular Vesicles. *International journal of molecular sciences* **19** (2018).

68. Takasugi, N. *et al.* TMEM30A is a candidate interacting partner for the β-carboxyl-terminal fragment of amyloid-β precursor protein in endosomes. *PloS one* **13**, e0200988-e0200988 (2018).
69. Haqqani, A.S. *et al.* Method for isolation and molecular characterization of extracellular microvesicles released from brain endothelial cells. *Fluids and barriers of the CNS* **10**, 4-4 (2013).
70. Chiasserini, D. *et al.* Proteomic analysis of cerebrospinal fluid extracellular vesicles: a comprehensive dataset. *Journal of proteomics* **106**, 191-204 (2014).

Figure 1

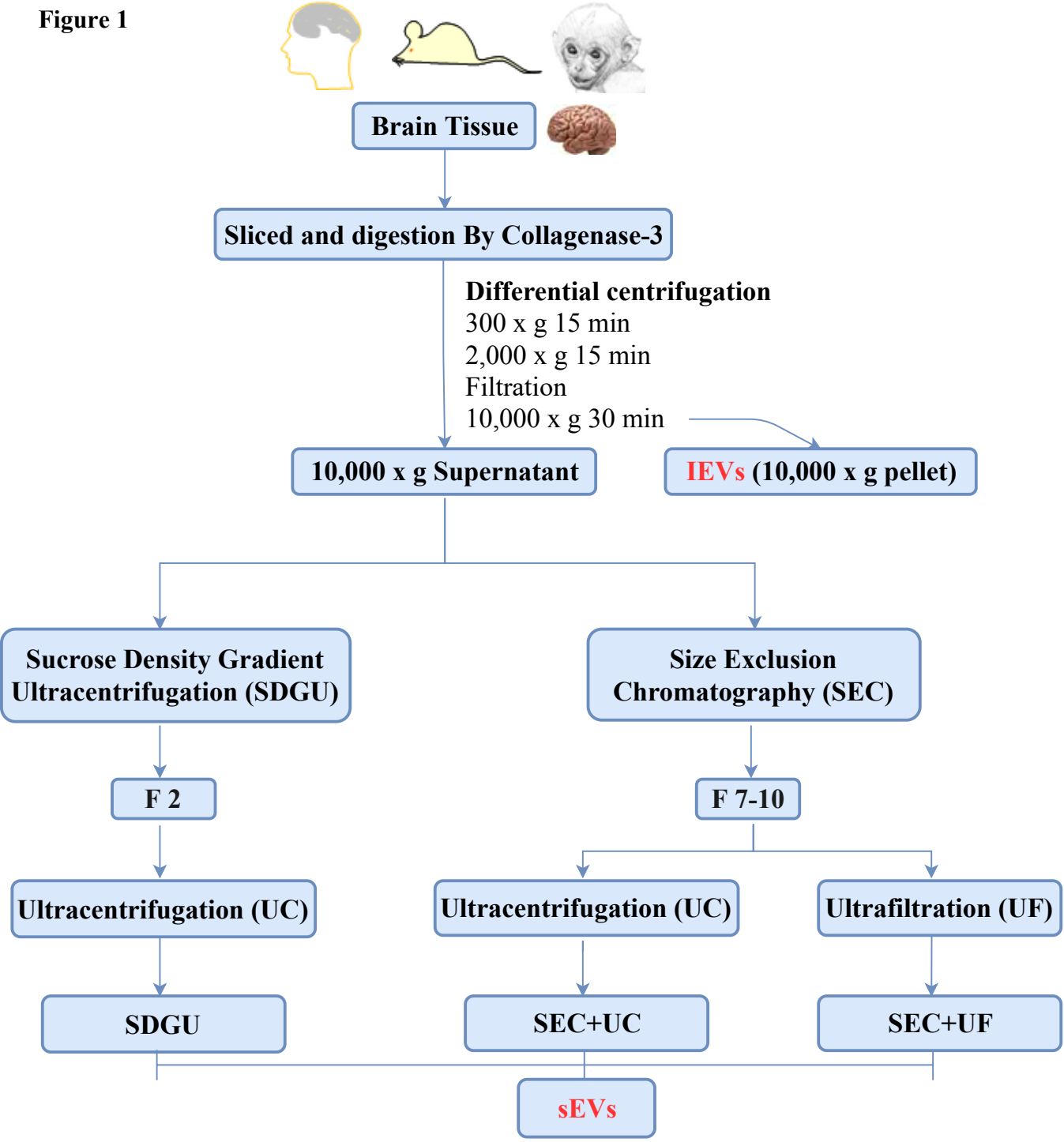
Brain Tissue
Sliced and digestion By Collagenase-3
Differential centrifugation
300 x g 15 min
2,000 x g 15 min
Filtration
10,000 x g 30 min
10,000 x g Supernatant
IEVs (10,000 x g pellet)
Sucrose Density Gradient Ultracentrifugation (SDGU)
Size Exclusion Chromatography (SEC)
F 2
F 7-10
Ultracentrifugation (UC)
Ultracentrifugation (UC)
Ultrafiltration (UF)
SDGU
SEC+UC
SEC+UF
sEVs

Figure 2

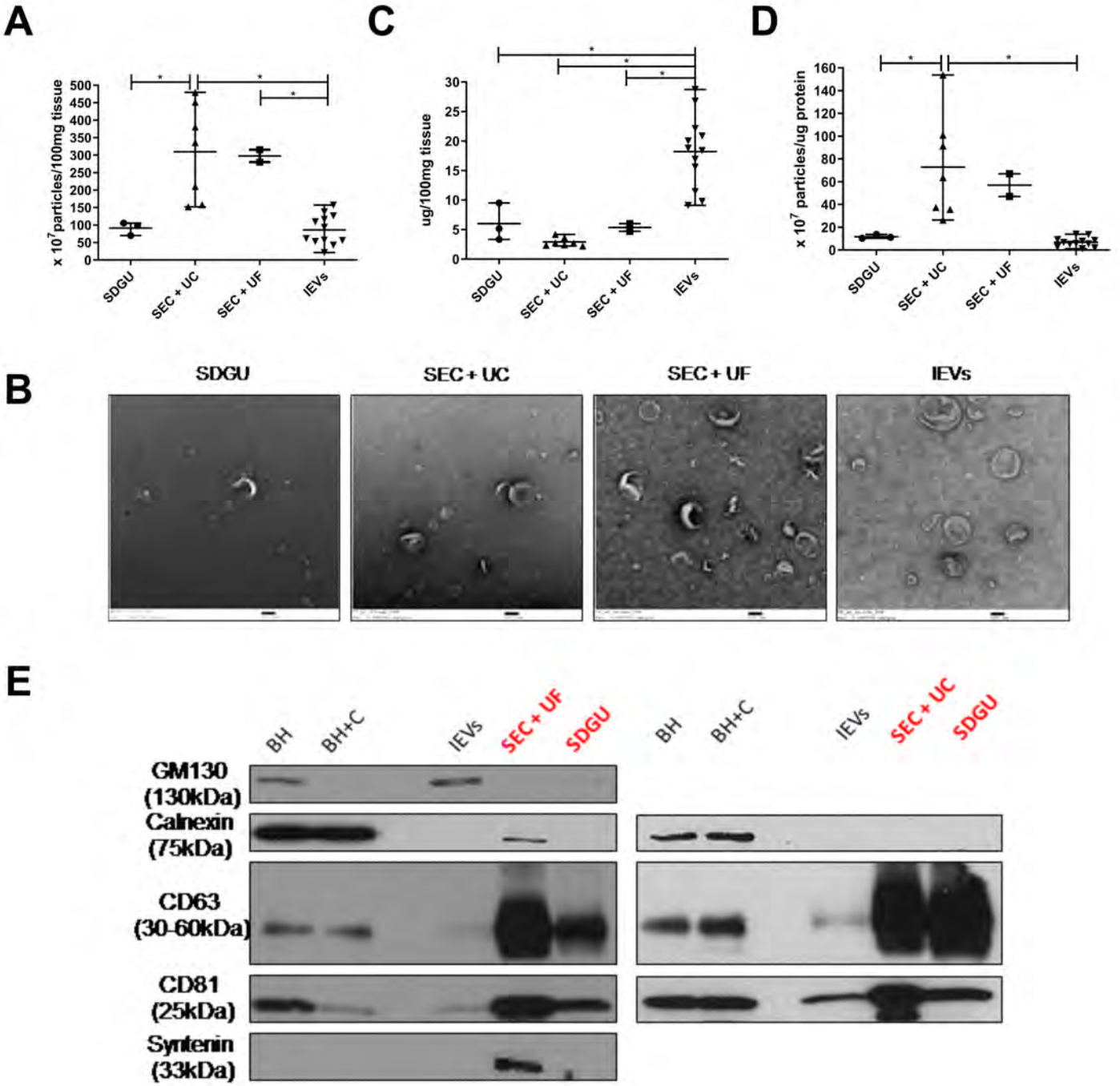
A
x 10^7 particles/100mg tissue
500
450
400
350
300
250
200
150
100
50
0
SDGU
SEC + UC
SEC + UF
IEVs
C
ug/100mg tissue
30
25
20
15
10
5
0
D
x 10^7 particles/ug protein
160
140
120
100
80
60
40
20
0
B
SDGU
SEC + UC
SEC + UF
IEVs
E
BH
BH+C
IEVs
SEC + UF
SDGU
BH
BH+C
IEVs
SEC + UC
SDGU
GM130
(130kDa)
Calnexin
(75kDa)
CD63
(30-60kDa)
CD81
(25kDa)
Syntenin
(33kDa)

Figure 3

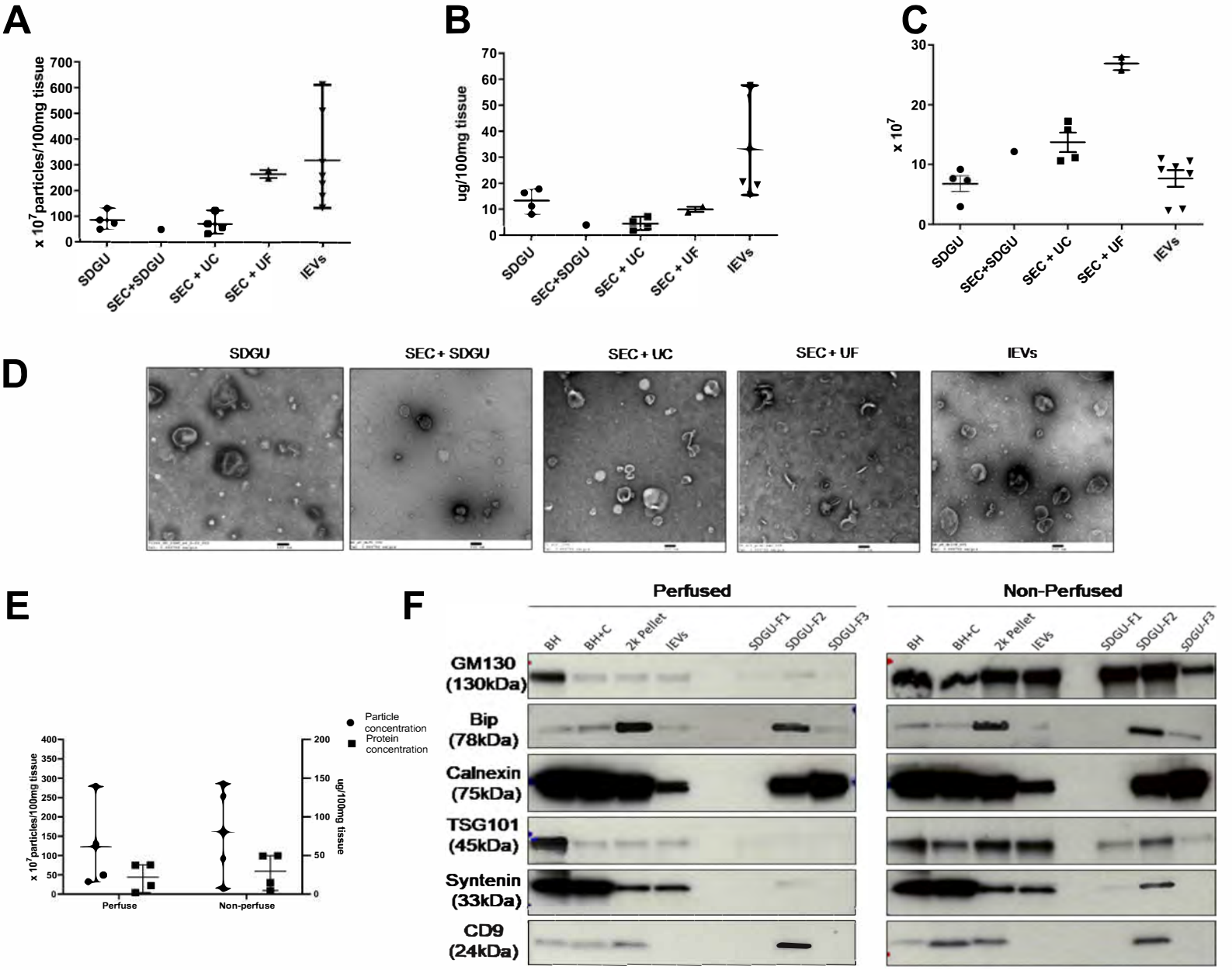
A
x 10^7 particles/100mg tissue
SDGU
SEC+SDGU
SEC + UC
SEC + UF
IEVs
B
ug/100mg tissue
C
x 10^7
D
SDGU
SEC + SDGU
SEC + UC
SEC + UF
IEVs
E
Particle concentration
Protein concentration
x 10^7 particles/100mg tissue
ug/100mg tissue
Perfuse
Non-perfuse
F
Perfused
Non-Perfused
BH
BH+C
2k Pellet
IEVs
SDGU-F1
SDGU-F2
SDGU-F3
GM130 (130kDa)
Bip (78kDa)
Calnexin (75kDa)
TSG101 (45kDa)
Syntenin (33kDa)
CD9 (24kDa)

Figure 4

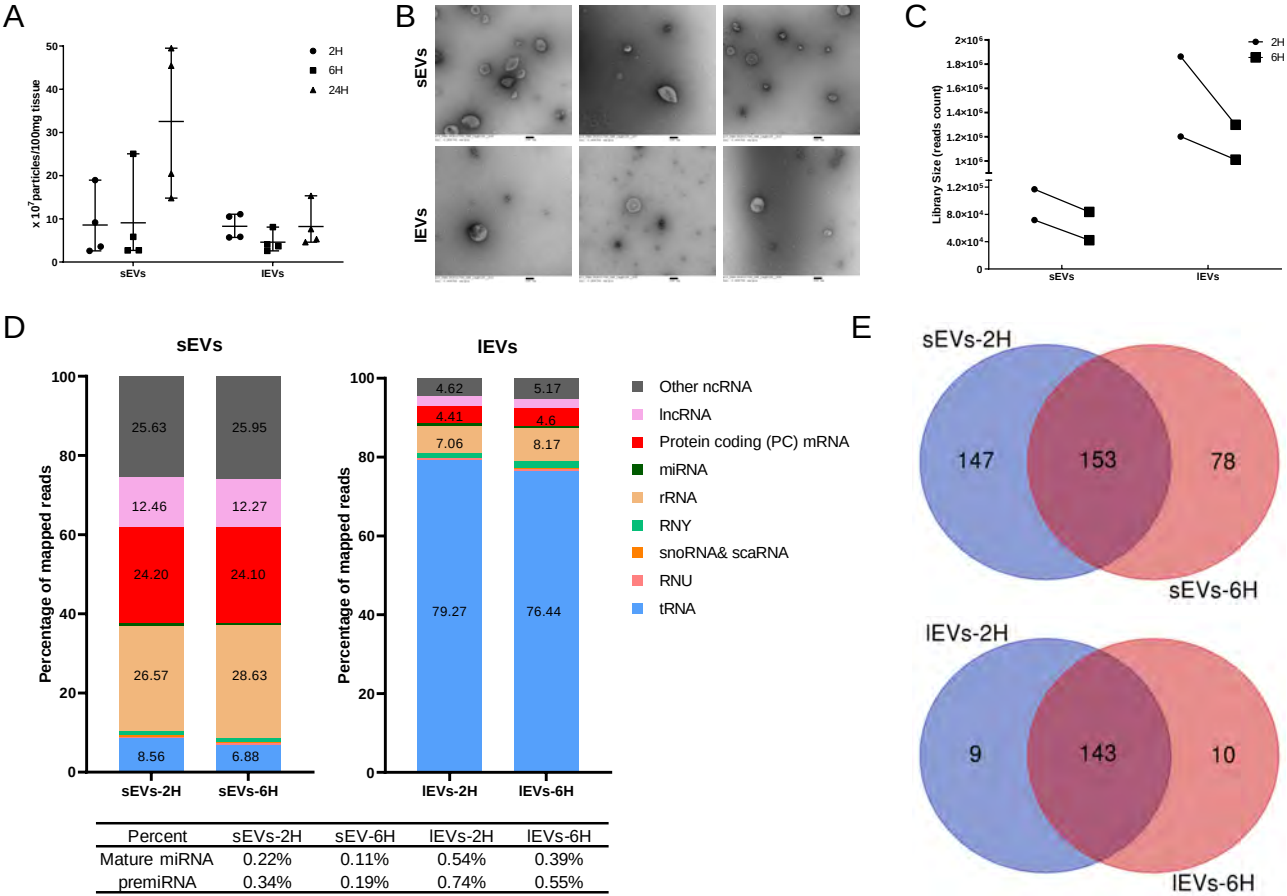

Percent	sEVs-2H	sEV-6H	lEVs-2H	lEVs-6H
Mature miRNA	0.22%	0.11%	0.54%	0.39%
premiRNA	0.34%	0.19%	0.74%	0.55%

Figure 5

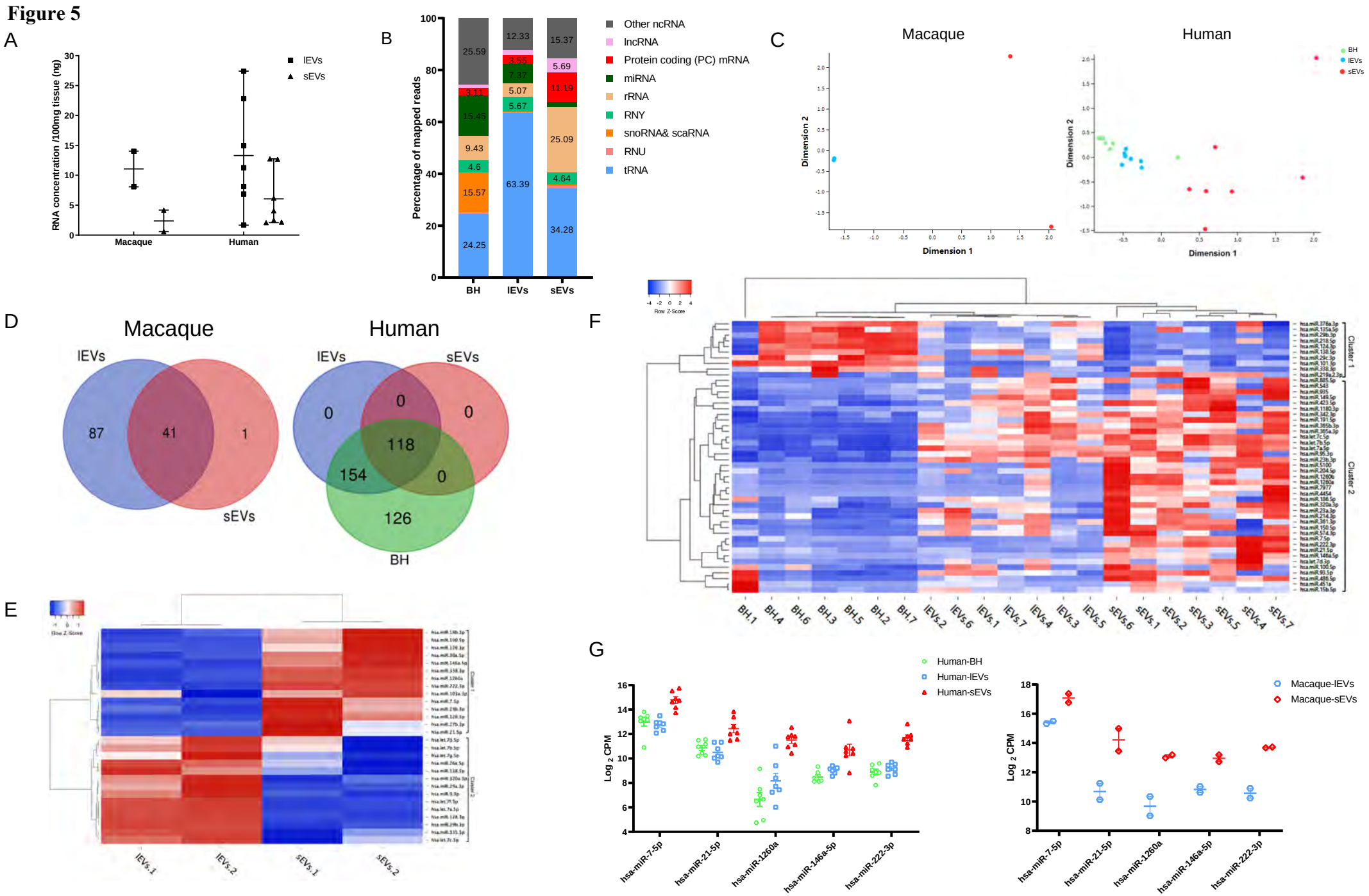
A
RNA concentration /100mg tissue (ng)
IEVs
sEVs
Macaque
Human
B
Percentage of mapped reads
BH
IEVs
sEVs
Other ncRNA
lncRNA
Protein coding (PC) mRNA
miRNA
rRNA
RNY
snoRNA& scaRNA
RNU
tRNA
C
Macaque
Human
Dimension 1
Dimension 2
D
Macaque
Human
IEVs
sEVs
BH
E
F
Cluster 1
Cluster 2
G
Human-BH
Human-IEVs
Human-sEVs
Macaque-IEVs
Macaque-sEVs
Log 2 CPM
hsa-miR-7-5p
hsa-miR-21-5p
hsa-miR-1260a
hsa-miR-146a-5p
hsa-miR-222-3p

Figure 6

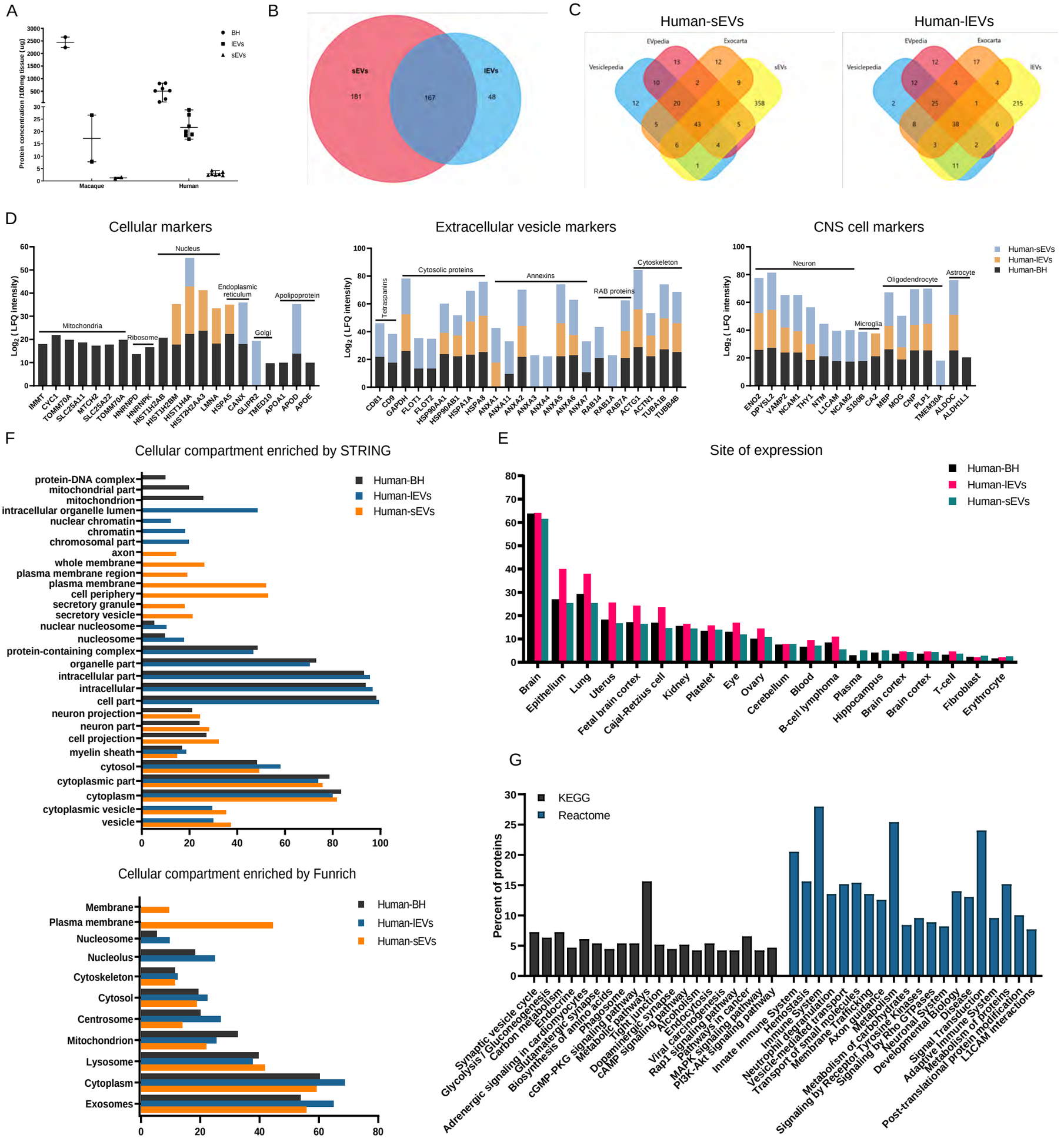
A
Protein concentration /100mg tissue (ug)
BH
lEVs
sEVs
Macaque
Human
B
sEVs
lEVs
181
167
48
C
Human-sEVs
Human-lEVs
EVpedia
Exocarta
Vesiclepedia
sEVs
lEVs
D
Cellular markers
Extracellular vesicle markers
CNS cell markers
Log2 (LFQ intensity)
Mitochondria
Ribosome
Nucleus
Endoplasmic reticulum
Golgi
Apolipoprotein
Tetraspanins
Cytosolic proteins
Annexins
RAB proteins
Cytoskeleton
Neuron
Microglia
Oligodendrocyte
Astrocyte
Human-sEVs
Human-lEVs
Human-BH
IMMT
CYC1
TOMM70A
SLC25A11
MTCH2
SLC25A22
TOMM70A
HNRNPD
HNRNPK
HIST1H2AB
HIST1H2BM
HIST1H4A
HIST2H2AA3
LMNA
HSPA5
CANX
GLIPR2
TMED10
APOA1
APOD
APOE
CD81
CD9
GAPDH
FLOT1
FLOT2
HSP90AA1
HSP90AB1
HSPA1A
HSPA8
ANXA1
ANXA11
ANXA2
ANXA3
ANXA4
ANXA5
ANXA6
ANXA7
RAB14
RAB1A
RAB7A
ACTG1
ACTN1
TUBA1B
TUBB4B
ENO2
DPYSL2
VAMP2
NCAM1
THY1
NTM
L1CAM
NCAM2
S100B
CA2
MBP
MOG
CNP
PLP1
TMEM30A
ALDOC
ALDH1L1
F
Cellular compartment enriched by STRING
Human-BH
Human-lEVs
Human-sEVs
protein-DNA complex
mitochondrial part
mitochondrion
intracellular organelle lumen
nuclear chromatin
chromatin
chromosomal part
axon
whole membrane
plasma membrane region
plasma membrane
cell periphery
secretory granule
secretory vesicle
nuclear nucleosome
nucleosome
protein-containing complex
organelle part
intracellular part
intracellular
cell part
neuron projection
neuron part
cell projection
myelin sheath
cytosol
cytoplasmic part
cytoplasm
cytoplasmic vesicle
vesicle
Cellular compartment enriched by Funrich
Membrane
Plasma membrane
Nucleosome
Nucleolus
Cytoskeleton
Cytosol
Centrosome
Mitochondrion
Lysosome
Cytoplasm
Exosomes
E
Site of expression
Human-BH
Human-lEVs
Human-sEVs
Brain
Epithelium
Lung
Uterus
Fetal brain cortex
Cajal-Retzius cell
Kidney
Platelet
Eye
Ovary
Cerebellum
Blood
B-cell lymphoma
Plasma
Hippocampus
Brain cortex
Brain cortex
T-cell
Fibroblast
Erythrocyte
G
KEGG
Reactome
Percent of proteins
Synaptic vesicle cycle
Glycolysis / Gluconeogenesis
Adrenergic signaling in cardiomyocytes
Carbon metabolism
Endocrine
Glutamatergic synapse
Biosynthesis of amino acids
Phagosome
cGMP-PKG signaling pathway
Metabolic pathways
Tight junction
Dopaminergic synapse
cAMP signaling pathway
Alcoholism
Endocytosis
Viral carcinogenesis
Rap1 signaling pathway
Pathways in cancer
MAPK signaling pathway
PI3K-Akt signaling pathway
Innate Immune System
Hemostasis
Immune System
Neutrophil degranulation
Vesicle-mediated transport
Transport of small molecules
Membrane Trafficking
Axon guidance
Metabolism
Metabolism of carbohydrates
Signaling by Receptor Tyrosine Kinases
Neuronal System
Signaling by Rho GTPases
Developmental Biology
Disease
Signal Transduction
Adaptive Immune System
Metabolism of proteins
Post-translational protein modification
L1CAM interactions

Figure S1

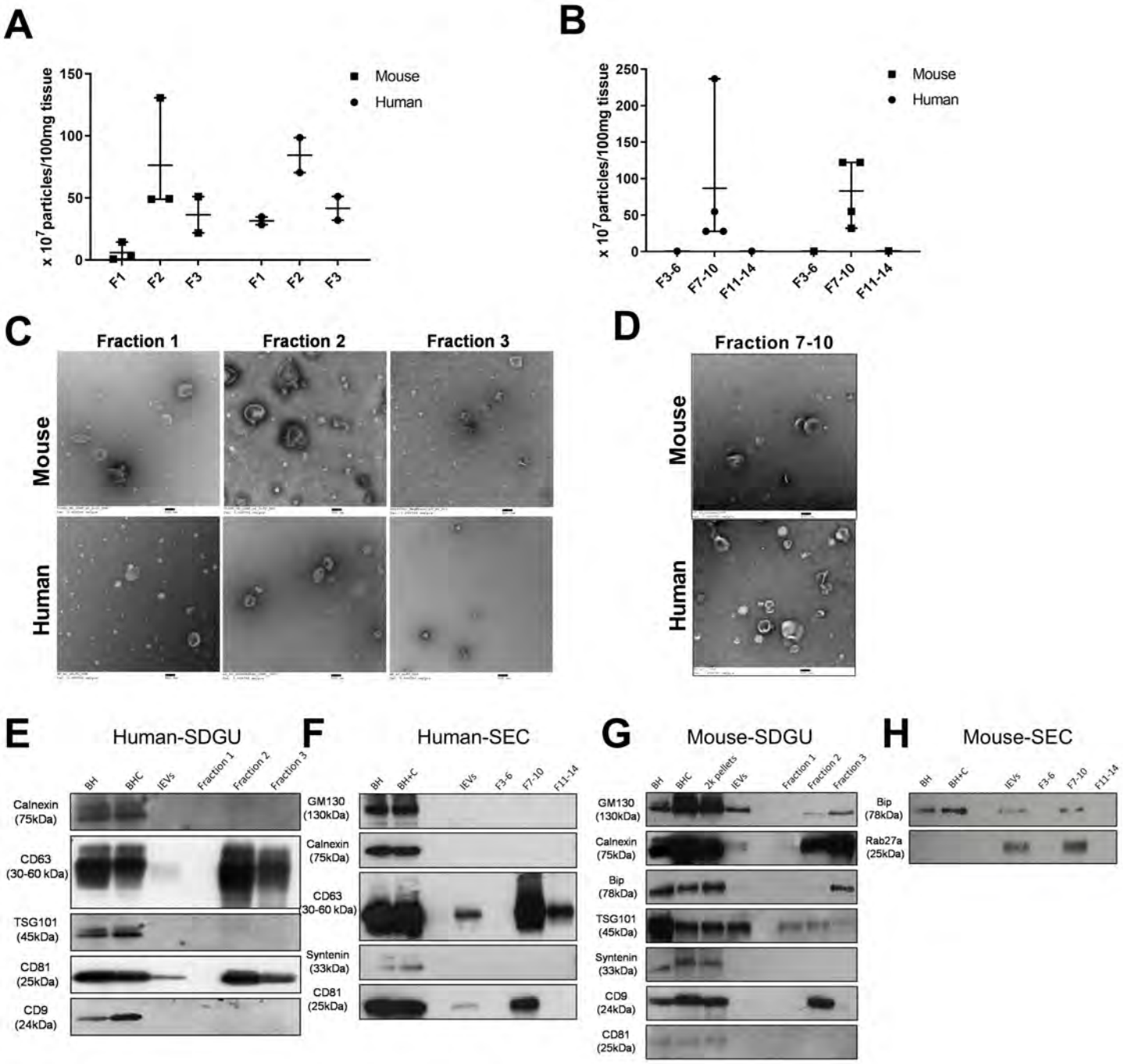
A
x 10^7 particles/100mg tissue
150
100
50
0
Mouse
Human
F1
F2
F3
F1
F2
F3
B
x 10^7 particles/100mg tissue
250
200
150
100
50
0
Mouse
Human
F3-6
F7-10
F11-14
F3-6
F7-10
F11-14
C
Fraction 1
Fraction 2
Fraction 3
Mouse
Human
D
Fraction 7-10
Mouse
Human
E
Human-SDGU
BH
BHC
IEVs
Fraction 1
Fraction 2
Fraction 3
Calnexin (75kDa)
CD63 (30-60 kDa)
TSG101 (45kDa)
CD81 (25kDa)
CD9 (24kDa)
F
Human-SEC
BH
BH+C
IEVs
F3-6
F7-10
F11-14
GM130 (130kDa)
Calnexin (75kDa)
CD63 (30-60 kDa)
Syntenin (33kDa)
CD81 (25kDa)
G
Mouse-SDGU
BH
BHC
2k pellets
IEVs
Fraction 1
Fraction 2
Fraction 3
GM130 (130kDa)
Calnexin (75kDa)
Bip (78kDa)
TSG101 (45kDa)
Syntenin (33kDa)
CD9 (24kDa)
CD81 (25kDa)
H
Mouse-SEC
BH
BH+C
IEVs
F3-6
F7-10
F11-14
Bip (78kDa)
Rab27a (25kDa)

Figure S2

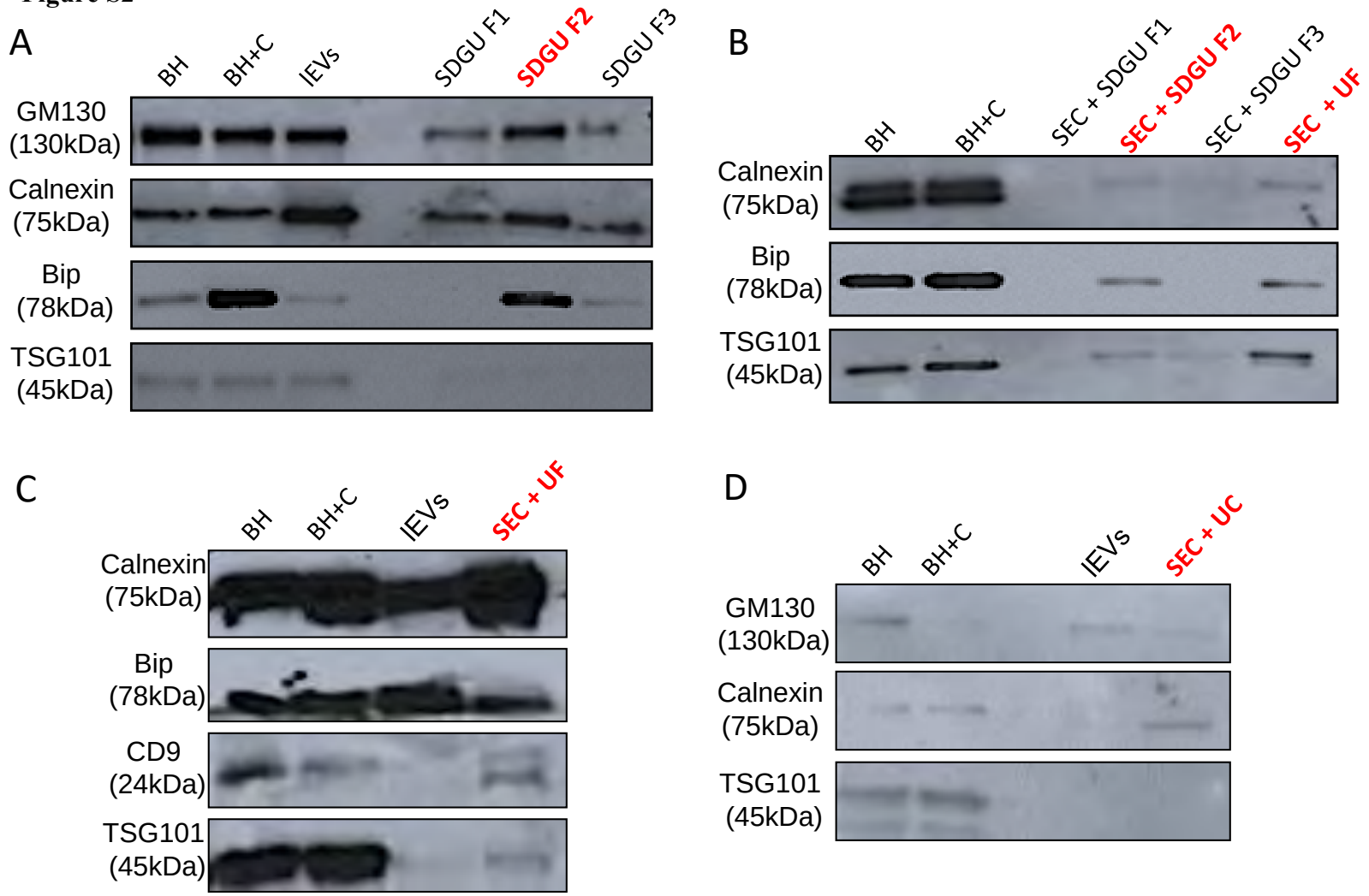
A
BH
BH+C
lEVs
SDGU F1
SDGU F2
SDGU F3
GM130
(130kDa)
Calnexin
(75kDa)
Bip
(78kDa)
TSG101
(45kDa)
B
BH
BH+C
SEC + SDGU F1
SEC + SDGU F2
SEC + SDGU F3
SEC + UF
Calnexin
(75kDa)
Bip
(78kDa)
TSG101
(45kDa)
C
BH
BH+C
lEVs
SEC + UF
Calnexin
(75kDa)
Bip
(78kDa)
CD9
(24kDa)
TSG101
(45kDa)
D
BH
BH+C
lEVs
SEC + UC
GM130
(130kDa)
Calnexin
(75kDa)
TSG101
(45kDa)

Figure S3

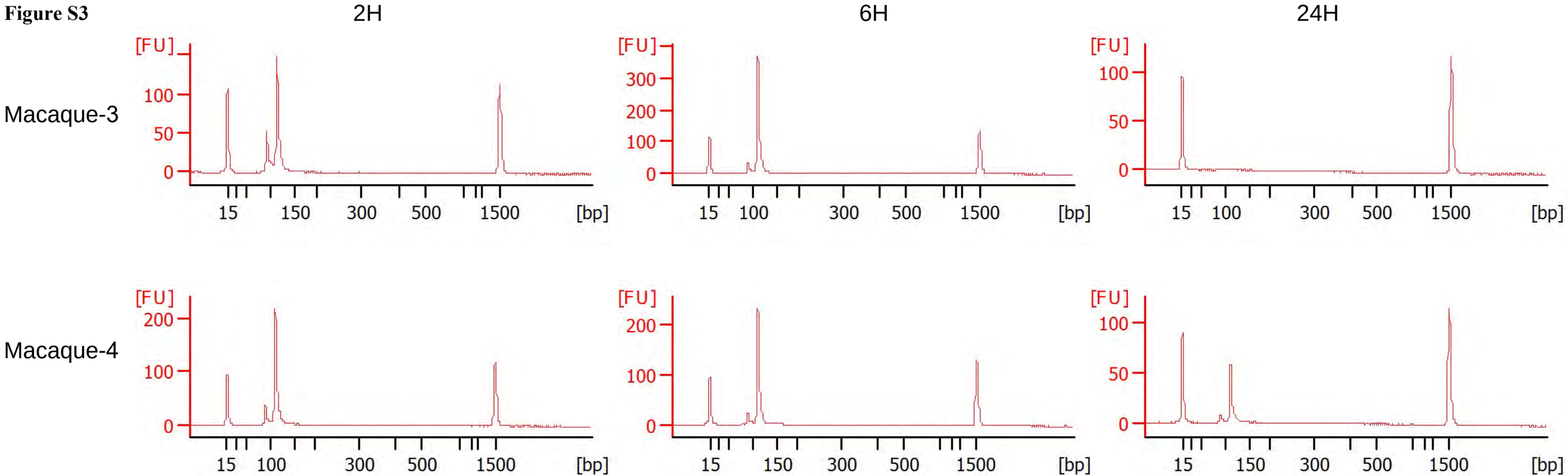
2H
6H
24H
Macaque-3
Macaque-4
[FU]
[bp]
15
150
100
300
500
1500
0
50
100
200
300

Figure S4

A

Protein number	sEVs	lEVs	BH
2H	51	23	1358
6H	71	50	1343
24H	184	76	1286

B

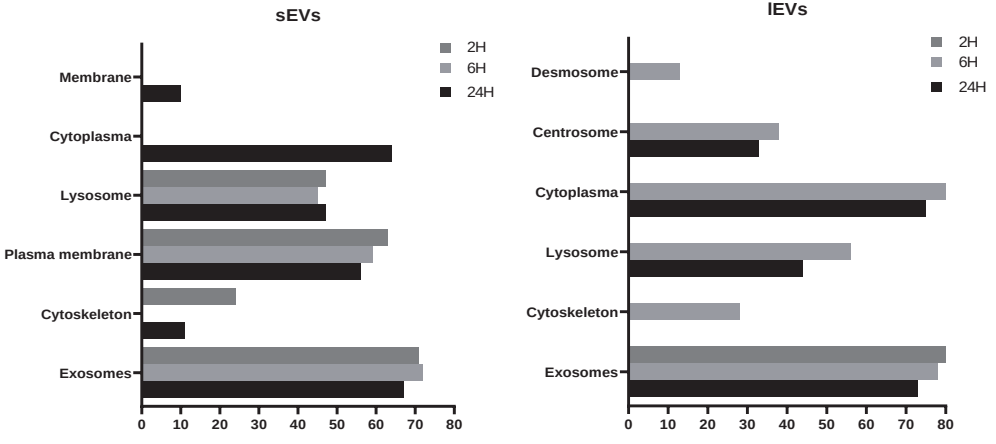
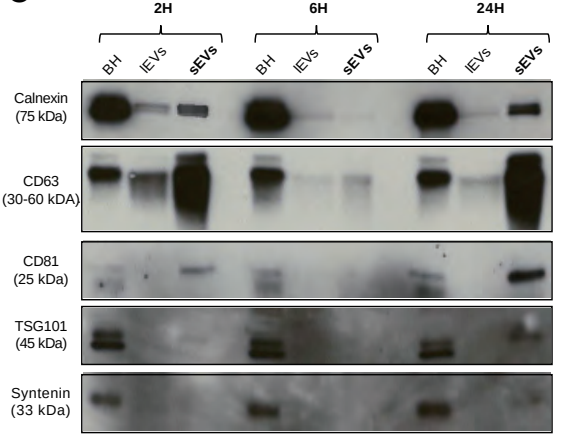
C